

CERN-PH-EP/2013-037
2016/02/09

CMS-TOP-14-021

Observation of top quark pairs produced in association with a vector boson in pp collisions at $\sqrt{s} = 8$ TeV

The CMS Collaboration*

Abstract

Measurements of the cross sections for top quark pairs produced in association with a W or Z boson are presented, using 8 TeV pp collision data corresponding to an integrated luminosity of 19.5 fb^{-1} , collected by the CMS experiment at the LHC. Final states are selected in which the associated W boson decays to a charged lepton and a neutrino or the Z boson decays to two charged leptons. Signal events are identified by matching reconstructed objects in the detector to specific final state particles from $t\bar{t}W$ or $t\bar{t}Z$ decays. The $t\bar{t}W$ cross section is measured to be $382_{-102}^{+117} \text{ fb}$ with a significance of 4.8 standard deviations from the background-only hypothesis. The $t\bar{t}Z$ cross section is measured to be $242_{-55}^{+65} \text{ fb}$ with a significance of 6.4 standard deviations from the background-only hypothesis. These measurements are used to set bounds on five anomalous dimension-six operators that would affect the $t\bar{t}W$ and $t\bar{t}Z$ cross sections.

Published in the Journal of High Energy Physics as doi:10.1007/JHEP01(2016)096.

1 Introduction

Since the LHC at CERN achieved proton-proton collisions at center-of-mass energies of 7 and 8 TeV, it has become possible to study signatures at significantly higher mass scales than ever before. The two heaviest sets of particles produced in standard model (SM) processes that could be observed using the data already collected are top quark pairs produced in association with a W or Z boson ($t\bar{t}W$ and $t\bar{t}Z$), which have expected cross sections of $\sigma(t\bar{t}W) = 203_{-22}^{+20}$ fb and $\sigma(t\bar{t}Z) = 206_{-24}^{+19}$ fb in the SM in 8 TeV collisions [1]. The dominant production mechanisms for $t\bar{t}W$ and $t\bar{t}Z$ in pp collisions are shown in Fig. 1. The $t\bar{t}Z$ production cross section provides the most accessible direct measurement of the top quark coupling to the Z boson. Both $\sigma(t\bar{t}W)$ and $\sigma(t\bar{t}Z)$ would be altered in a variety of new physics models that can be parameterized by dimension-six operators added to the SM Lagrangian.

The $t\bar{t}Z$ cross section was first measured by the CMS experiment in 7 TeV collisions, with a precision of about 50% [2]. Measurements in events containing three or four leptons in 8 TeV collisions at CMS [3] have constrained $\sigma(t\bar{t}Z)$ to within 45% of its SM value, and yielded evidence of $t\bar{t}Z$ production at 3.1 standard deviations from the background-only hypothesis. The CMS collaboration also used same-sign dilepton events to constrain $\sigma(t\bar{t}W)$ to within 70% of the SM prediction, with a significance of 1.6 standard deviations from the background-only hypothesis. Most recently, the ATLAS experiment used events containing two to four leptons to measure $\sigma(t\bar{t}W) = 369_{-91}^{+100}$ fb at 5.0 standard deviations from the background-only hypothesis, and $\sigma(t\bar{t}Z) = 176_{-52}^{+58}$ fb with a significance of 4.2 standard deviations from the background-only hypothesis [4].

We present the first observation of $t\bar{t}Z$ production and measurements of the $t\bar{t}W$ and $t\bar{t}Z$ cross sections using a full reconstruction of the top quarks and the W or Z boson from their decay products. We target events in which the associated W boson decays to a charged lepton and a neutrino ($W \rightarrow \ell\nu$) or the Z boson decays to two charged leptons ($Z \rightarrow \ell\ell$). In this paper, “lepton” (ℓ) refers to an electron, a muon, or a τ lepton decaying into other leptons. The top quark pair may decay into final states with hadronic jets ($t\bar{t} \rightarrow bq\bar{q}\bar{b}q\bar{q}$), a lepton plus jets ($t\bar{t} \rightarrow b\ell\nu\bar{b}q\bar{q}$), or two leptons ($t\bar{t} \rightarrow b\ell\nu\bar{b}\ell\nu$). The $t\bar{t}Z$ process is measured in channels with two, three, or four leptons, with exactly one pair of same-flavor opposite-sign leptons with an invariant mass close to the Z boson mass [5]. The $t\bar{t}W$ process is measured in channels with two same-sign leptons or three leptons, where no lepton pair is consistent with coming from a Z boson decay. Additional b-tagged jets and light flavor jets are required to enable full or partial reconstruction of the top quark and W boson decays.

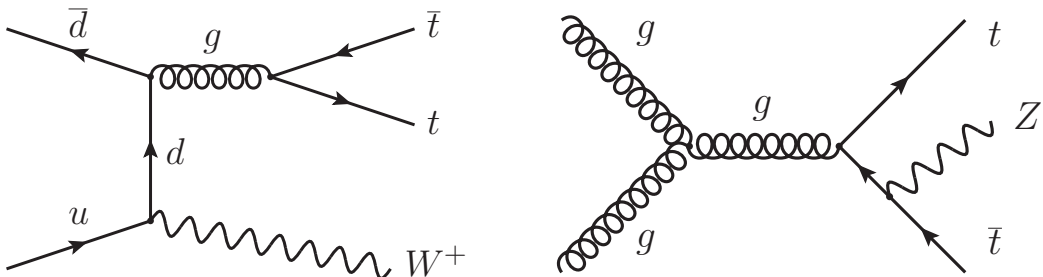


Figure 1: Dominant leading order Feynman diagrams for $t\bar{t}W^+$ and $t\bar{t}Z$ production at the LHC. The charge conjugate process of $t\bar{t}W^+$ produces $t\bar{t}W^-$.

Channels defined by lepton charge and multiplicity are further subdivided by lepton flavor and the number of jets, in order to provide an initial separation between signal and background (Section 5). Background processes with leptons from W and Z boson decays are estimated using Monte Carlo simulations that are validated in separate control regions (Section 6.1). Processes

with leptons from other sources are estimated directly from the data, using events in which one or more leptons fail to satisfy a strict set of selection criteria (Sections 6.2 and 6.3). In each channel, we attempt a full or partial reconstruction of the $t\bar{t}W$ or $t\bar{t}Z$ system with a linear discriminant that matches leptons and jets to their parent particles using mass, charge, and b tagging information (Section 7). Additional kinematic variables from leptons and jets are combined with output from the linear discriminant in a multivariate analysis that is used to make the final measurement of the $t\bar{t}W$ and $t\bar{t}Z$ cross sections (Sections 8 and 10). Finally, the measured cross sections are used to constrain the coupling of the top quark to the Z boson, and to set bounds on five anomalous dimension-six operators (Section 11).

2 The CMS detector

The central feature of the CMS apparatus is a superconducting solenoid of 6 m internal diameter, providing a magnetic field of 3.8 T. Within the solenoid volume are a silicon pixel and strip tracker, a lead tungstate crystal electromagnetic calorimeter (ECAL), and a brass and scintillator hadron calorimeter (HCAL), each composed of a barrel and two endcap sections. Extensive forward calorimetry complements the coverage provided by the barrel and endcap detectors. Muons are detected in gas-ionization muon chambers embedded in the steel flux-return yoke outside the solenoid.

A global event description is obtained using the CMS particle-flow (PF) algorithm [6, 7], which combines information from all CMS sub-detectors to reconstruct and identify individual particles in collision events. The particles are placed into mutually exclusive classes: charged hadrons, neutral hadrons, photons, muons, and electrons. The primary collision vertex is identified as the reconstructed vertex with the highest value of $\sum p_T^2$, where p_T is the momentum component transverse to the beams, and the sum is over all the charged particles used to reconstruct the vertex. The energy of photons is directly obtained from the ECAL measurement, corrected for zero-suppression effects. The energy of electrons is determined from a combination of the electron momentum at the primary interaction vertex as determined by the tracker, the energy of the corresponding ECAL cluster, and the energy sum of all bremsstrahlung photons spatially compatible with originating from the electron track. The energy of muons is obtained from the curvature of the corresponding track and hits in the muon chambers. The energy of charged hadrons is determined from a combination of their momentum measured in the tracker and the matching ECAL and HCAL energy deposits, corrected for zero-suppression effects and for the response function of the calorimeters to hadronic showers. Finally, the energy of neutral hadrons is obtained from the corresponding corrected ECAL and HCAL energy.

A more detailed description of the CMS detector, together with a definition of the coordinate system used and the relevant kinematic variables, can be found in Ref. [8].

3 Data and simulated samples

This search is performed with an integrated luminosity of $19.5 \pm 0.5 \text{ fb}^{-1}$ of proton-proton collisions at $\sqrt{s} = 8 \text{ TeV}$, collected in 2012 [9]. Dilepton triggers were used to collect data for all channels. The dilepton triggers require any combination of electrons and muons, where one lepton has $p_T > 17 \text{ GeV}$ and another has $p_T > 8 \text{ GeV}$. A trielectron trigger with minimum p_T thresholds of 15, 8, and 5 GeV was also used for channels with three or more leptons. These triggers approach their maximum efficiency for leptons with p_T values at least 2 GeV higher than the thresholds.

Expected signal events and some of the background processes are modeled with simulation. The signal processes $t\bar{t}W$ and $t\bar{t}Z$, as well as background processes producing a single Z boson, WZ , ZZ , $W^\pm W^\pm$, WWW , WWZ , $t\bar{t}$, $t\bar{t}\gamma$, $t\bar{t}\gamma^*$, $t\bar{t}WW$, and the associated production of a Z boson with a single top quark ($t\bar{t}Z$), are all generated with the MADGRAPH 5.1.3 [10] tree-level matrix element generator, combined with PYTHIA 6.4 [11] for the parton shower and hadronization. The associated production of a Higgs boson with a top quark pair ($t\bar{t}H$) is modeled using the PYTHIA generator assuming a Higgs boson mass of 125 GeV. Samples that include top quark production are generated with a top quark mass of 172.5 GeV. The CTEQ6L1 parton distribution function (PDF) set [12] is used for all samples.

The CMS detector response is simulated using GEANT4 software [13]. Both data and simulated events are required to pass the same trigger requirements and are reconstructed with identical algorithms. Effects from additional proton-proton collisions in the same bunch crossing (pileup) in the simulation are modeled by adding simulated inclusive proton-proton interactions (generated with PYTHIA) to the generated hard collision, with the pileup interaction multiplicity in simulation reflecting the profile inferred from data. Correction factors are applied to individual objects and events to bring object properties and efficiencies in simulation into better agreement with data, as described in Section 4.

4 Object reconstruction and identification

Certain types of particles reconstructed with the PF algorithm are particularly useful in identifying and reconstructing $t\bar{t}W$ and $t\bar{t}Z$ events. These objects are electrons, muons, charged and neutral hadrons clustered into jets, and the imbalance in \vec{p}_T arising from neutrinos in the event.

Electrons with $p_T > 10$ GeV are reconstructed over the full pseudorapidity range of the tracker, $|\eta| < 2.5$. The reconstruction combines information from clusters of energy deposits in the ECAL and the electron trajectory reconstructed in the inner tracker [14, 15]. A multivariate analysis technique combines observables sensitive to the amount of bremsstrahlung, spatial and momentum matching between the track and associated ECAL clusters, and shower shape observables, to distinguish genuine electrons from charged hadrons [14].

Muons with $|\eta| < 2.4$ and $p_T > 10$ GeV are reconstructed using information from both the silicon tracker and the muon spectrometer [16]. Track candidates must have a minimum number of tracker hits, be compatible with hits in the muon chambers, and match the associated energy deposits in the calorimeters, to be selected as PF muons [17].

The τ leptons decay before reaching the ECAL, and are not identified in this analysis. Their decay products are instead identified as hadrons, which may be clustered into jets, or as electrons or muons, depending on whether the τ lepton decays to hadrons or leptons.

Prompt leptons (electrons or muons from a W, Z, or Higgs boson, or the decay of a τ lepton) are distinguished from non-prompt leptons (misidentified jets or leptons from hadron decays) in part by assessing their isolation from surrounding hadronic activity. Lepton isolation is calculated by summing the p_T of other particles in a cone of radius $\Delta R = \sqrt{(\Delta\eta)^2 + (\Delta\phi)^2} = 0.4$ around the lepton direction, where $\Delta\eta$ and $\Delta\phi$ are the pseudorapidity and azimuthal angle difference (in radians) from the lepton direction. Contributions from charged particles not originating from the primary collision vertex are subtracted from the isolation sum, multiplied by a factor of 1.5 to account for the neutral pileup contribution [18]. The relative isolation of the lepton is defined as the ratio of the corrected isolation sum to the lepton p_T .

Prompt leptons are also identified by having low impact parameter (IP) and impact parameter

significance (S_{IP}) values, where the impact parameter is the minimum three-dimensional distance between the lepton trajectory and the primary vertex, and its significance is the ratio of the IP value to its uncertainty. (These values tend to be higher for electrons and muons from the decay of τ leptons, which have a nonnegligible lifetime.) Furthermore, the properties of the nearest jet enclosing the lepton (within $\Delta R < 0.5$) can be used to identify non-prompt leptons. The ratio of the lepton p_{T} to the p_{T} of this enclosing jet tends to be lower for non-prompt leptons. Also, an enclosing jet identified as coming from a bottom quark indicates that the lepton is likely non-prompt and originates from a b-hadron decay.

Three levels of lepton selection are defined: preselected, loose, and tight. The preselection includes leptons in data sidebands used to compute non-prompt backgrounds, the loose criteria select signal leptons in channels dominated by prompt lepton events, and the tight selection is used when the largest backgrounds contain non-prompt leptons. Loose leptons form a subset of the preselected leptons, and tight leptons form a subset of the loose leptons. The selection requirements are described below and summarized in Table 1.

The preselection removes leptons with an enclosing jet identified as a bottom jet, as described below, and imposes very loose requirements on the distance from the lepton trajectory to the primary vertex in the z direction and in the x - y plane, and on the S_{IP} value. Preselected leptons must also have a relative isolation less than 0.4. The preselection has $\approx 100\%$ efficiency for prompt leptons, and accepts a substantial number of non-prompt leptons. Loose leptons must lie below certain thresholds on the relative isolation calculated using only charged particles (0.15 for electrons and 0.20 for muons), and loose muons pass a tighter requirement on S_{IP} . The loose selection retains 93–99% of prompt muons and 89–96% of prompt electrons, depending on p_{T} and η , and rejects $\approx 50\%$ of non-prompt leptons that pass the preselection. Tight leptons must pass several selection criteria: the charged relative isolation must be less than 0.05 for electrons and 0.10 for muons; the ratio of lepton to enclosing jet p_{T} must be more than 0.6; and for electrons, the IP must be less than 0.15 mm. The tight selection efficiency is $\approx 90\%$ for prompt muons and $\approx 80\%$ for prompt electrons, with efficiency ranges of 68–98% for muons and 49–93% for electrons, depending on p_{T} and η . The tight selection rejects $\approx 80\%$ of non-prompt muons and $\approx 85\%$ of non-prompt electrons that pass the preselection.

In order to reject leptons with misreconstructed charge, the preselected, loose, and tight leptons in some channels must pass additional charge identification (ID) requirements. Electrons must pass a veto on electrons from photon conversions and have no missing hits in the inner tracker, and muons must have more than five inner tracker hits. Electrons must also have the same charge assignment from the tracker and from the relative location of ECAL energy deposits from the electron itself and from its bremsstrahlung radiation. This charge ID selection efficiency ranges from 85 to 100% for tight electrons with correctly identified charge, depending on p_{T} and η , while more than 97% of electrons with misreconstructed charge are rejected. The charge ID selection has 99% efficiency for tight muons with correctly identified charge and rejects $\approx 100\%$ of muons with misreconstructed charge. Lepton selection efficiencies are measured using same-flavor (SF) lepton pairs with an invariant mass near the Z boson mass. The charge ID selection requirements are summarized in Table 1.

Charged and neutral PF particles are clustered into jets using the anti- k_{T} algorithm with a distance parameter of 0.5 [19, 20]. Selected jets must be separated by $\Delta R > 0.5$ from the selected leptons, and have $p_{\text{T}} > 25 \text{ GeV}$ and $|\eta| < 2.4$. Charged PF particles not associated with the primary event vertex are removed from jet clustering, and additional requirements remove jets arising entirely from pileup vertices [21]. A neutral component is removed by applying a residual energy correction following the area-based procedure described in Refs. [22, 23], to account

Table 1: Summary of preselected, loose, tight, and charge ID lepton selection requirements. The charge ID requirements are applied in addition to the preselected, loose, or tight lepton criteria.

Lepton selection criteria	Preselected		Loose		Tight		Charge ID	
	e	μ	e	μ	e	μ	e	μ
p_T (GeV)	>10	>10	>10	>10	>10	>10		
$ \eta $	<2.5	<2.4	<2.5	<2.4	<2.5	<2.4		
Relative isolation	<0.4	<0.4	<0.4	<0.4	<0.4	<0.4		
Charged relative isolation			<0.15	<0.20	<0.05	<0.15		
Ratio of lepton p_T to jet p_T					>0.6	>0.6		
x - y distance to vertex (mm)	<5	<5	<5	<5	<5	<5		
z distance to vertex (mm)	<10	<10	<10	<10	<10	<10		
$ \text{IP} $ (mm)					<0.15			
S_{IP}	<10	<10	<10	<4	<10	<4		
Inner tracker hits								>5
Missing inner tracker hits	<2		<2		<2		0	
Tracker charge – ECAL charge							0	
Electron conversion veto							Pass	

for pileup activity. Fake jets from instrumental effects are rejected by requiring each jet to have at least two PF constituents and at least 1% of its energy from ECAL and HCAL deposits.

The combined secondary vertex (CSV) algorithm [24, 25] is used to identify (or “tag”) jets originating from a bottom quark. The CSV algorithm utilizes information about the impact parameter of tracks and reconstructed secondary vertices within the jets to assign each jet a discriminator, with higher values indicating a likely b-quark origin. For a selection with the medium working point of the CSV discriminator, the b tagging efficiency is around 70% (20%) for jets originating from a bottom quark (charm quark), and the chance of mistagging jets from light quarks or gluons is about 1%. For the loose working point, the efficiency to tag jets from b quarks (c quarks) is approximately 85% (40%), and the probability to tag jets from light quarks or gluons is about 10%. These efficiencies and mistag probabilities vary with the p_T and η of the jets.

The missing transverse momentum vector, arising from the presence of undetected neutrinos in the event, is calculated as the negative vector sum of the \vec{p}_T of all PF candidates in the event. This vector is denoted as \vec{p}_T^{miss} , and its magnitude as p_T^{miss} . Since pileup interactions can cause missing transverse momentum not associated with the primary interaction, the magnitude of the negative vector sum of the \vec{p}_T of only selected jets and leptons (H_T^{miss}) is also used. The H_T^{miss} variable has worse resolution than p_T^{miss} , but it is more robust as it does not rely on low- p_T objects in the event.

The simulation is corrected with data-to-simulation scale factors in order to match the performance of reconstructed objects in data. Simulated events with leptons are corrected for trigger efficiency, as well as for lepton identification and isolation efficiency. Scale and resolution corrections accounting for residual differences between data and simulation are applied to the muon and electron momenta. All lepton corrections are derived from samples with a Z boson or J/ψ decaying into two leptons. Jet energy corrections based on simulation and on γ +jets, Z+jets, and dijet data are applied as a function of the jet p_T and η [26]. Separate scale factors ranging from 0.6 to 2.0 are applied to light and heavy flavor jets to correct the distribution of CSV values [27].

5 Event selection

Events for this analysis are divided into five mutually exclusive channels, targeting different decay modes of the $t\bar{t}W$ and $t\bar{t}Z$ systems. For all channels, at least one lepton is required to have $p_T > 20$ GeV, and the remaining leptons must have $p_T > 10$ GeV, to satisfy the dilepton trigger requirements. In addition, to reject leptons from Y , J/ψ , and off-shell photon decays, no pair of leptons can have an invariant mass less than 12 GeV. The selection requirements for each channel are described below and summarized in Table 2.

Table 2: Summary of selection requirements for each channel.

Channel	OS $t\bar{t}Z$		SS $t\bar{t}W$			3ℓ $t\bar{t}W$		3ℓ $t\bar{t}Z$		4ℓ $t\bar{t}Z$	
Lepton flavor	$ee/\mu\mu$	$e\mu$	ee	$e\mu$	$\mu\mu$	Any		Any		Any	
Lepton ID	2 loose		2 tight			SS tight		SS tight		4 loose	
Lepton charge ID	≥ 0 pass		2 pass			SS pass		SS pass		4 pass	
$Z \rightarrow \ell\ell$ candidates	1		0			0		≥ 1		2	1
Number of jets	5	≥ 6	3	≥ 4		1	≥ 2	3	≥ 4	≥ 1	
Number of b tags	≥ 1 medium		≥ 2 loose or ≥ 1 medium						≥ 1 loose		
Other			$Z \rightarrow ee$ veto							$H_T^{\text{miss}} > 30$ GeV	
Subchannels	4		6			2		2		2	

The opposite-sign (OS) dilepton channel targets $t\bar{t}Z$ events where the Z boson decays into an OS pair of electrons or muons, and the $t\bar{t}$ system decays hadronically. We select events with loose OS leptons forming an invariant mass within 10 GeV of the Z boson mass and at least five jets, where one or more jets pass the medium CSV working point. The channel is split into categories with SF lepton pairs (targeting events with a Z boson) and different-flavor pairs (to calibrate the $t\bar{t}$ background). It is further subdivided into events with exactly five jets and those with six or more jets, which have a higher signal-to-background ratio. This categorization provides an initial separation of the $t\bar{t}Z$ signal from the dominant Z boson and $t\bar{t}$ backgrounds, which are estimated from simulation.

The same-sign (SS) dilepton channel selects $t\bar{t}W$ events in which the associated W boson, and the W boson of the same charge from the $t\bar{t}$ system, each decay to a lepton and a neutrino, and the remaining W boson decays to quarks. Events are selected with two SS tight leptons which pass the charge ID criteria, plus three or more jets, of which at least two pass the loose CSV threshold or at least one passes the medium CSV threshold. In addition, in dielectron events, the ee invariant mass must be at least 10 GeV away from the Z boson mass, to reject Z boson decays in which the charge of one electron is misidentified. This channel is divided by lepton flavor (ee , $e\mu$, and $\mu\mu$), and further into categories with exactly three jets and four or more jets. The dominant background is $t\bar{t}$ with one non-prompt lepton, which is estimated from data by computing a misidentification rate. Diboson WZ events (modeled with simulation) are selected if one lepton from the Z boson decay does not pass the preselection, or if the Z boson decays to a pair of τ leptons, of which only one produces a muon or electron. For the ee and $e\mu$ categories, dileptonic Z boson and $t\bar{t}$ events with a charge-misidentified electron also appear in the final selection.

The three-lepton (3ℓ) $t\bar{t}W$ channel targets events in which both the associated W and the pair of W bosons from the $t\bar{t}$ pair decay leptonically. Events are selected in which the lepton charges add up to ± 1 , and the two leptons of the same charge pass the tight identification and the charge ID criteria. Furthermore, no SF OS pair of leptons can have a mass within 10 GeV of the Z boson mass. Events must have at least one medium b-tagged jet, or at least two loose

b-tagged jets, and are divided into categories with exactly one jet, or with two or more jets. The main backgrounds are $t\bar{t}$ decays with a non-prompt lepton, estimated from data, and WZ events, estimated using simulation.

The 3ℓ $t\bar{t}Z$ channel selects events in which the Z boson decays to a pair of electrons or muons, and one W boson from the $t\bar{t}$ system decays to a charged lepton and a neutrino, with the remaining W boson decaying to quarks. The selection is identical to the one used for the 3ℓ $t\bar{t}W$ channel, except that at least one SF OS pair of leptons must have an invariant mass within 10 GeV of the Z boson mass, and the categories have exactly three jets, or four or more jets. The dominant backgrounds are Z boson and $t\bar{t}$ events with a non-prompt lepton, and WZ events with prompt leptons, estimated in the same manner as in the 3ℓ $t\bar{t}W$ channel.

Events with four leptons (4ℓ) come from $t\bar{t}Z$ decays in which the Z boson and both W bosons decay leptonically. This channel requires four leptons that pass the loose identification and the charge ID, and whose charges add up to zero. At least one SF OS dilepton pair must have a mass within 10 GeV of the Z boson mass, and at least one loose b-tagged jet must be present. In addition, H_T^{miss} must exceed 30 GeV. These criteria, and the categorization of events into those with exactly one lepton pair consistent with a Z boson decay, and those with two or more, help separate $t\bar{t}Z$ events from the dominant ZZ background, which is estimated using simulation. Small backgrounds from $t\bar{t}$, WZ, and Z boson events with one or two non-prompt leptons are also estimated using simulation.

6 Signal and background modeling

Events in the signal channels fall into three broad categories. Signal and “prompt” background events have enough leptons from W or Z boson decays, with the correct charges, to satisfy the lepton selection of the channel. “Non-prompt” backgrounds have at least one lepton which is a jet misidentified as an electron, or which comes from the in-flight decay of a hadron, or from photon conversion. The “charge misidentified” background has an electron whose charge was misidentified. The expected yields for these processes after the final selection are shown in Tables 3–5 in Section 6.4.

6.1 Signal and prompt backgrounds

The signal and prompt backgrounds are estimated using simulation, normalized to their predicted inclusive cross sections. We use next-to-next-to-leading-order (NNLO) cross sections for $t\bar{t}$ [28] and single Z boson [29] production; next-to-leading-order (NLO) cross sections for $t\bar{t}W$ and $t\bar{t}Z$ [1], $t\bar{t}H$ [30], $t\bar{t}\gamma$ [10, 31], WZ and ZZ [32], and WWW, WWZ, and $t\bar{t}Z$ [10] production; and leading-order cross sections for $W^\pm W^\pm$, $t\bar{t}\gamma^*$, and $t\bar{t}WW$ [10] production. Additional corrections are derived from data for Z boson, WZ, and ZZ processes with multiple extra jets.

Rare processes such as SS diboson ($W^\pm W^\pm$) and triboson production (WWW, WWZ), associated production of a Z boson with a single top quark ($t\bar{t}Z$), and $t\bar{t}$ with an on-shell or off-shell photon ($t\bar{t}\gamma/t\bar{t}\gamma^*$) or two W bosons ($t\bar{t}WW$) are subdominant backgrounds. The associated production of a Higgs boson with a top quark pair is included as a background, with uncertainties derived from theoretical predictions. All of these are minor backgrounds, with fewer expected events than the signal in each channel.

The main prompt backgrounds are $t\bar{t}$ and Z boson production (in the OS dilepton channel), WZ events (in the SS and 3ℓ channels), and ZZ events (in the 3ℓ and 4ℓ channels). Because the Z boson, WZ, and ZZ simulation samples are produced with fewer extra partons from QCD radiation than there are jets in the final selection, their estimated contributions to the signal

channels are approximations with large uncertainties. To get a more accurate estimate of these yields, scale factors are derived from events with SF OS leptons consistent with a Z boson decay and no medium b-tagged jets. Using about 5000 data events, of which 97% are expected to come from $Z \rightarrow \ell\ell$ events, we correct the predicted yield from the Z boson simulation as a function of the number of jets for events with five or more jets. To validate this technique, we derive a scale factor from four jet events with no medium b tags and apply it to events with at least one medium b tag, and find that it yields good agreement between data and the Z boson simulation. These scale factors range from 1.35 to 1.7, and each has an uncertainty of 30%, based on the level of data-to-simulation agreement in Z boson events with four jets. Additional uncertainties in the η distribution of jets in Z boson and $t\bar{t}$ events, and on the p_T^{miss} distribution in Z boson events with extra jets, are assessed due to possible data-to-simulation discrepancies in OS dilepton events with four or more jets (excluding the OS $t\bar{t}Z$ signal region). Scale factors for simulated WZ and ZZ events with three or more jets are derived from 80 three-lepton data events (70% from WZ) with no medium b-tagged jets and at most one loose b-tagged jet. The scale factors of 1.4 for three-jet events, and 1.6 for events with four or more jets, have 40% and 60% uncertainties, respectively, based on the limited number of 3ℓ data events used to derive the scale factors.

In addition, there is significant uncertainty associated with the simulation of events with extra heavy flavor partons. Simulated $t\bar{t}$, WZ, and ZZ events with one or two extra c jets, an extra b jet, or two extra b jets are separated from their inclusive samples and assigned extra rate uncertainties of 50%. The single Z boson simulation is divided similarly. However, by comparing the expected and observed numbers of b-tagged jets in SF OS events with low p_T^{miss} and exactly four jets, we are able to constrain the uncertainty in each of the Z boson plus heavy flavor jet processes to 30%.

The top quark p_T spectrum in $t\bar{t}$ simulation (from MADGRAPH) is corrected to agree with the distribution predicted by higher-order calculations [33] and observed in $t\bar{t}$ differential cross section measurements in $\sqrt{s} = 8$ TeV data, using the techniques described in Ref. [34].

6.2 Non-prompt backgrounds

Backgrounds with at least one non-prompt lepton are expected to have larger yields than the signal in the SS and 3ℓ $t\bar{t}W$ channels, about the same yields in the 3ℓ $t\bar{t}Z$ channel, and very low yields in the 4ℓ channel. Non-prompt backgrounds in the SS and 3ℓ channels are estimated from data. A sideband region dominated by non-prompt processes is defined by events which pass the same selection as the signal channels, but in which one or both of the preselected SS leptons fail the tight lepton criteria. Extrapolation to the signal region is performed by weighting the sideband events by the probability for non-prompt leptons to pass the tight lepton selection (the misidentification rate, ϵ). Events in which one of the SS leptons fails the tight lepton requirement enter the signal region estimate with weight $\epsilon/(1 - \epsilon)$. Events where both SS leptons fail the tight lepton selection get a negative weight $-\epsilon_1\epsilon_2/[(1 - \epsilon_1)(1 - \epsilon_2)]$; this accounts for events with two non-prompt leptons contaminating the sideband sample of events with a single non-prompt lepton.

The misidentification rate is measured with SS and 3ℓ data events, separately for electrons and muons, and as a function of the lepton p_T . Same-sign dilepton events with two or more jets (excluding the $t\bar{t}W$ signal region) are dominated by $t\bar{t}$ decays with a non-prompt lepton. Three-lepton events with two or fewer jets, a lepton pair consistent with a Z boson decay, and low p_T^{miss} come mostly from Z boson production with an extra non-prompt lepton. These events usually have exactly one prompt and one non-prompt SS lepton, so we use a modified tag-

and-probe approach in which the prompt lepton is tagged with the tight lepton selection, and the fraction of preselected probe leptons passing the tight selection measures ϵ . Because both leptons in the numerator of this ratio are tight, there is a $\approx 50\%$ chance that the tag lepton was actually non-prompt, and the probe lepton was prompt. We estimate the size of this contamination by weighting events where the tag lepton fails the tight selection by $\epsilon/(1-\epsilon)$, and subtract those with a tight probe lepton from the numerator, and those with a preselected probe from the denominator.

Since this correction term depends on ϵ itself, we cannot solve for ϵ explicitly. Instead, we find the set of p_T - and flavor-dependent ϵ values that minimizes the difference between the data and predicted yields in the SS and 3ℓ derivation regions, binned by lepton p_T and flavor. Events in which both SS leptons are non-prompt naturally cancel to zero with the correction term, while those with two prompt SS leptons are estimated from simulation and subtracted explicitly. The misidentification rate in all the p_T bins is computed to be $\approx 20\%$ for muons and $\approx 15\%$ for electrons, except for the muon bin with $p_T > 30$ GeV, whose rate is 36%. This rate is uncorrelated with variables that do not depend on the lepton flavor or p_T , including most of those used to separate signal from background events (Section 8). The relative uncertainty in ϵ is assessed at 40% for electrons and 60% for muons, equal to the maximum observed discrepancy between predicted and observed yields in any of 20 background-dominated selection regions with two SS leptons and two or more jets, or three leptons and two or fewer jets. There is an additional statistical uncertainty of 50% for leptons with medium p_T and 100% for leptons with high p_T , due to low event yields in the ϵ derivation regions.

In the 4ℓ channel, there are too few events passing the kinematic requirements to use a data sideband to model the non-prompt background. Instead we use simulated WZ, Z boson, and $t\bar{t}$ samples to estimate non-prompt yields after the final selection, which are expected to be much smaller than the signal yields. We derive a scale factor for the simulation estimate of non-prompt leptons passing the loose selection using simulated Z boson and $t\bar{t}$ events with exactly three loose leptons and one or two jets, where at least one passes a medium b tag. Events with a SF OS lepton pair close to the Z boson mass are dominated by Z boson plus non-prompt lepton events; those without such a pair are dominated by $t\bar{t}$ plus non-prompt lepton events. The derived scale factor of 2.0 per non-prompt lepton is then applied to the simulation in the 4ℓ category, with 100% rate uncertainties.

6.3 Charge-misidentified backgrounds

The misidentified charge background in SS dilepton events is estimated from OS dilepton events in data that pass all the other signal channel selections, weighted by the probability for an electron passing the charge ID requirement to have misidentified charge. This probability is derived from data as a function of electron η from the ratio of SS dielectron events with an invariant mass within 10 GeV of the Z boson mass and zero or more jets, to OS events with the same selection. The probability ranges from 0.003% for central electrons to 0.1% for endcap electrons. The absence of a Z boson mass peak in SS dimuon events indicates that the probability is negligible for muons. Opposite-sign $e\mu$ events enter the SS prediction region with a weight equal to the probability for the electron to have its charge misidentified; ee events enter with the sum of the probabilities for each electron. The charge misidentification probability has a 30% rate uncertainty, based on the agreement between predicted and observed SS dielectron events with multiple jets and with the ee invariant mass close to the Z boson mass. We expect to see fewer events with charge misidentified electrons than $t\bar{t}W$ signal events in all the SS dilepton channels.

6.4 Expected yields

Expected yields for the signal and background processes after the final fit described in Section 10, along with the observed data yields, are shown in Tables 3–5.

Table 3: Expected yields after the final fit described in Section 10, compared to the observed data for OS $t\bar{t}Z$ final states. Here “hf” and “lf” stand for heavy and light flavors, respectively.

OS $t\bar{t}Z$	$e^\pm e^\mp / \mu^\pm \mu^\mp$		$e^\pm \mu^\mp$	
	5 jets	≥ 6 jets	5 jets	≥ 6 jets
Z+lf jets	265 ± 57	93 ± 20	<0.1	<0.1
Z+c \bar{c} jets	341 ± 74	106 ± 23	<0.1	<0.1
Z+b jet	236 ± 59	68 ± 18	<0.1	<0.1
Z+b \bar{b} jets	378 ± 72	136 ± 25	<0.1	<0.1
$t\bar{t}$ +lf jets	188 ± 19	58.4 ± 7.3	180 ± 16	57.8 ± 6.4
$t\bar{t}$ +hf jets	57 ± 16	30.6 ± 8.3	52 ± 15	27.3 ± 7.3
tbZ/ $t\bar{t}WW$	4.2 ± 1.8	1.8 ± 0.7	<0.1	<0.1
$t\bar{t}H$	1.4 ± 0.1	1.0 ± 0.2	1.0 ± 0.1	0.6 ± 0.1
Background total	1470 ± 135	494 ± 45	233 ± 21	85.8 ± 9.7
$t\bar{t}Z$	24.0 ± 5.5	28.2 ± 6.8	1.3 ± 0.3	0.8 ± 0.2
$t\bar{t}W$	1.1 ± 0.2	0.5 ± 0.1	1.2 ± 0.2	0.8 ± 0.2
Expected total	1495 ± 135	523 ± 45	236 ± 21	87.4 ± 9.7
Data	1493	526	251	78

Table 4: Expected yields after the final fit described in Section 10, compared to the observed data for SS $t\bar{t}W$ final states. The multiboson process includes WWW, WWZ, and $W^\pm W^\pm$; $t\bar{t}+X$ includes $t\bar{t}\gamma$, $t\bar{t}\gamma^*$, and $t\bar{t}WW$.

SS $t\bar{t}W$	$e^\pm e^\pm$		$e^\pm \mu^\pm$		$\mu^\pm \mu^\pm$	
	3 jets	≥ 4 jets	3 jets	≥ 4 jets	3 jets	≥ 4 jets
Non-prompt	16.0 ± 3.7	12.9 ± 3.1	57.0 ± 5.4	40.5 ± 4.2	29.0 ± 4.7	26.0 ± 4.4
Charge-misidentified	3.3 ± 1.6	1.7 ± 0.8	2.9 ± 0.7	1.6 ± 0.4	—	—
WZ	1.6 ± 0.5	0.9 ± 0.3	4.5 ± 1.4	2.2 ± 0.8	3.1 ± 1.0	1.3 ± 0.5
ZZ	0.2 ± 0.1	0.1 ± 0.1	0.3 ± 0.1	0.2 ± 0.1	0.2 ± 0.1	0.1 ± 0.1
Multiboson	0.8 ± 0.3	0.5 ± 0.2	1.5 ± 0.5	1.2 ± 0.4	1.2 ± 0.5	1.1 ± 0.4
tbZ/ $t\bar{t}+X$	1.4 ± 0.4	2.5 ± 1.3	4.1 ± 1.4	5.8 ± 2.2	0.9 ± 0.3	1.2 ± 0.4
$t\bar{t}H$	0.3 ± 0.1	1.4 ± 0.2	1.1 ± 0.1	4.0 ± 0.5	0.7 ± 0.1	3.0 ± 0.5
Background total	23.7 ± 4.1	20.1 ± 3.5	71.4 ± 5.8	55.4 ± 4.9	35.1 ± 4.8	32.8 ± 4.5
$t\bar{t}W$	5.5 ± 1.4	8.1 ± 1.9	13.9 ± 3.7	25.2 ± 5.5	10.4 ± 2.8	17.7 ± 4.0
$t\bar{t}Z$	0.4 ± 0.1	1.3 ± 0.3	1.1 ± 0.2	3.0 ± 0.6	0.7 ± 0.1	2.1 ± 0.4
Expected total	29.6 ± 4.4	29.4 ± 4.0	86.4 ± 6.9	83.6 ± 7.3	46.2 ± 5.6	52.6 ± 6.0
Data	31	32	89	69	47	61

7 Full event reconstruction

Even after the selection requirements have been applied, the final signal categories are dominated by background events. To help identify the $t\bar{t}W$ and $t\bar{t}Z$ signals, and the $t\bar{t}$ background, we attempt a full reconstruction of the events, by matching leptons, jets, and p_T^{miss} to the decaying W and Z bosons, and to the top quark and antiquark.

In all channels targeting the $t\bar{t}Z$ signal, the SF OS pair of leptons with an invariant mass closest to the Z boson mass is assumed to be from the Z boson decay. In selected $t\bar{t}W$ events, there

Table 5: Expected yields after the final fit described in Section 10, compared to the observed data for 3ℓ $t\bar{t}W$ and three and 4ℓ $t\bar{t}Z$ final states. The 4ℓ “Z-veto” channel has exactly one lepton pair consistent with a Z boson decay; the “Z” channel has two. The multiboson process includes WWW and WWZ; $t\bar{t}+X$ includes $t\bar{t}\gamma$, $t\bar{t}\gamma^*$, and $t\bar{t}WW$.

Process	3ℓ $t\bar{t}W$		3ℓ $t\bar{t}Z$		4ℓ $t\bar{t}Z$	
	1 jet	≥ 2 jets	3 jets	≥ 4 jets	≥ 1 jet+Z	≥ 1 jet+Z-veto
Non-prompt	44.6 ± 5.3	54.8 ± 6.4	8.2 ± 2.8	5.4 ± 2.1	—	—
Non-prompt WZ/Z	—	—	—	—	<0.1	<0.1
Non-prompt $t\bar{t}$	—	—	—	—	<0.1	0.2 ± 0.2
WZ	3.2 ± 0.8	8.0 ± 1.7	11.7 ± 2.9	5.4 ± 1.6	—	—
ZZ	1.0 ± 0.2	1.5 ± 0.3	1.6 ± 0.4	0.9 ± 0.3	3.3 ± 0.5	1.8 ± 0.3
Multiboson	0.1 ± 0.1	0.4 ± 0.2	0.5 ± 0.2	0.5 ± 0.2	<0.1	0.3 ± 0.1
$t\bar{b}Z/t\bar{t}+X$	0.4 ± 0.1	3.8 ± 1.1	1.6 ± 0.6	0.7 ± 0.3	<0.1	<0.1
$t\bar{t}H$	0.2 ± 0.1	4.7 ± 0.4	0.3 ± 0.1	0.4 ± 0.1	<0.1	0.2 ± 0.1
Background total	49.5 ± 5.4	73.1 ± 6.7	23.9 ± 4.1	13.3 ± 2.7	3.3 ± 0.5	2.4 ± 0.4
$t\bar{t}W$	2.5 ± 0.8	18.8 ± 4.7	0.5 ± 0.1	0.2 ± 0.1	—	—
$t\bar{t}Z$	0.3 ± 0.1	7.5 ± 1.2	8.8 ± 1.9	16.9 ± 3.6	0.4 ± 0.1	4.3 ± 1.0
Expected total	52.3 ± 5.4	99.4 ± 8.3	33.2 ± 4.5	30.4 ± 4.5	3.7 ± 0.5	6.7 ± 1.1
Data	51	97	32	30	3	6

are at least two leptons and two undetected neutrinos, so the associated W boson cannot be reconstructed. Thus, for both $t\bar{t}W$ and $t\bar{t}Z$ events, as well as $t\bar{t}$ events, it is the $t\bar{t}$ system which remains to be reconstructed. In selected OS $t\bar{t}Z$ events, both W bosons from the $t\bar{t}$ pair decay into quarks; we refer to this as a fully hadronic $t\bar{t}$ decay. In SS $t\bar{t}W$ and 3ℓ $t\bar{t}Z$ events, the $t\bar{t}$ pair decays semileptonically. The 3ℓ $t\bar{t}W$ and 4ℓ $t\bar{t}Z$ channels target leptonic $t\bar{t}$ decays. While background $t\bar{t}$ events have genuine top quarks to reconstruct, they decay in a different mode than the signal does, e.g. in OS $t\bar{t}$ events both W bosons decay leptonically, and in SS and 3ℓ $t\bar{t}$ events one lepton usually comes from a b-hadron decay.

The leptons, jets, and p_T^{miss} from $t\bar{t}$ decays preserve information about their parent particles. Pairs of jets from hadronic W boson decays have an invariant mass close to the W boson mass; adding the b jet from the same top quark decay gives three jets with an invariant mass close to the top quark mass. In semileptonic $t\bar{t}$ decays, the transverse component of the lepton momentum vector and \vec{p}_T^{miss} give a Jacobian mass distribution which peaks around 60 GeV and quickly drops as it approaches the W boson mass. Additionally, the lepton and b jet coming from the same top quark decay will have an invariant mass smaller than the top quark mass. Jets from b quarks tend to have higher CSV values, while light flavor jets have lower values, and c jets have an intermediate distribution. The jet charges of b jets from top quarks and quark jets from W boson decays are also used. Finally, the ratio of the invariant mass using only the transverse component of momentum vectors (M_T) to the full invariant mass tends to be higher for the set of jets coming from top quark and W boson decays than for sets with jets from extra radiated partons. These variables are all used in the event reconstruction described below, and are listed in Appendix A, Table 10.

To optimally match jets and leptons to their top quark and W boson parents in $t\bar{t}$ decays, we construct a linear discriminant, similar to a likelihood ratio, which evaluates different permutations of object-parent pairings. The discriminant is created using millions of simulated $t\bar{t}$ events, so the true parentage of each object is known, and the variable distribution shapes have high precision. For each input variable to the discriminant, we take the ratio of the distribution using correctly matched objects (e.g. the invariant mass of two jets coming from the same W

boson decay) to the distribution using any set of objects (e.g. the invariant mass of any two jets in the event), and rescaled the ratio histogram to have a mean value of one for correctly matched objects, as shown in Fig. 2. Variables with more discriminating power, such as the reconstructed W boson mass, have ratio histograms with some bin values very close to zero, and others above one; less discriminating variables such as b jet charge have values well above zero in all bins.

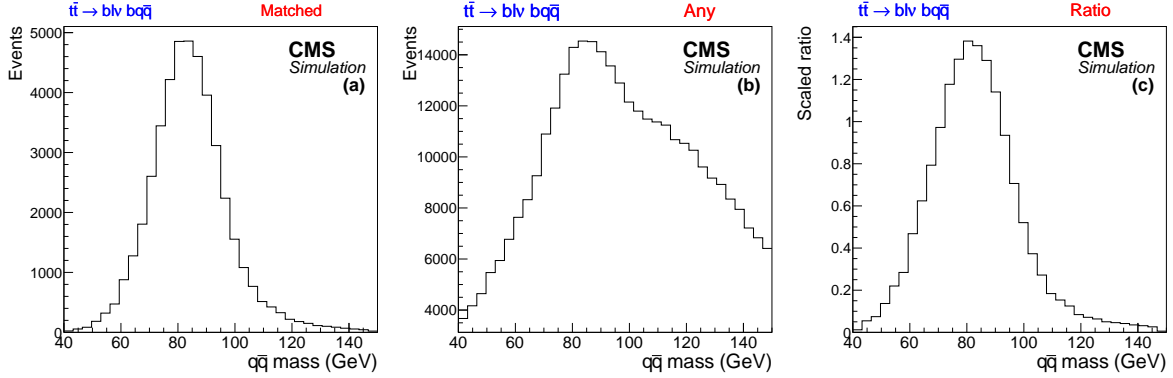


Figure 2: Distributions from simulated $t\bar{t} \rightarrow b\ell\nu\bar{b}q\bar{q}$ events with exactly four jets. Shown are the invariant mass of two jets matched to a hadronic W boson decay (a), the invariant mass of any two jets (b), and the rescaled ratio of the two (c).

We use these ratio histograms to match objects to $t\bar{t}$ decays in selected events in the $t\bar{t}W$ and $t\bar{t}Z$ signal regions, where the object parentage is not known. In $t\bar{t}Z$ channels the leptons matched to the Z boson decay are excluded from the $t\bar{t}$ reconstruction, and in $t\bar{t}W$ channels the lepton with the worst match to a $t\bar{t}$ decay is assumed to come from the associated W boson. For each permutation of leptons and jets matched to parent particles, we find the value of every variable (mass, CSV, charge, etc.) associated with an object-parent pairing. The matching discriminant is then computed as the product of the corresponding bin values from all the ratio histograms. The permutation with the highest discriminant value is considered to be the best reconstruction of the $t\bar{t}$ system. To more easily display the full range of values, we take the log of the discriminant value of the best reconstruction to calculate the match score. Events that contain all of the jets and leptons from the $t\bar{t}$ decay have match scores around zero, while events without all the decay products typically get negative scores. For semileptonic $t\bar{t}$ decays in events with exactly four jets, all from the $t\bar{t}$ system, the highest scored permutation is the correct assignment 75% of the time. For events with five or more jets, of which four are from the $t\bar{t}$ system, the exact correct match is achieved in 40% of cases, as there are five times as many permutations to choose from. Since one or two jets from the $t\bar{t}$ decay often fail to be reconstructed, we also attempt to match partial $t\bar{t}W$ and $t\bar{t}Z$ systems, with one or two jets missing. Output match scores in the OS $t\bar{t}Z$, SS $t\bar{t}W$, and 3ℓ $t\bar{t}Z$ channels are shown in Fig. 3, along with the 68% confidence level (CL) uncertainty in the signal plus background prediction.

Since the background processes do not have the same parent particles as the signal in each channel, their best reconstructed match scores are typically lower. Thus, the match scores for full or partial reconstructions of the $t\bar{t}$ system in $t\bar{t}W$, $t\bar{t}Z$, and $t\bar{t}$ decays, along with the values of input variables to the chosen match (e.g. dijet mass of the hadronically decaying W boson in a semileptonic $t\bar{t}$ decay), provide good discrimination between signal and background processes, especially those without any genuine top quarks.

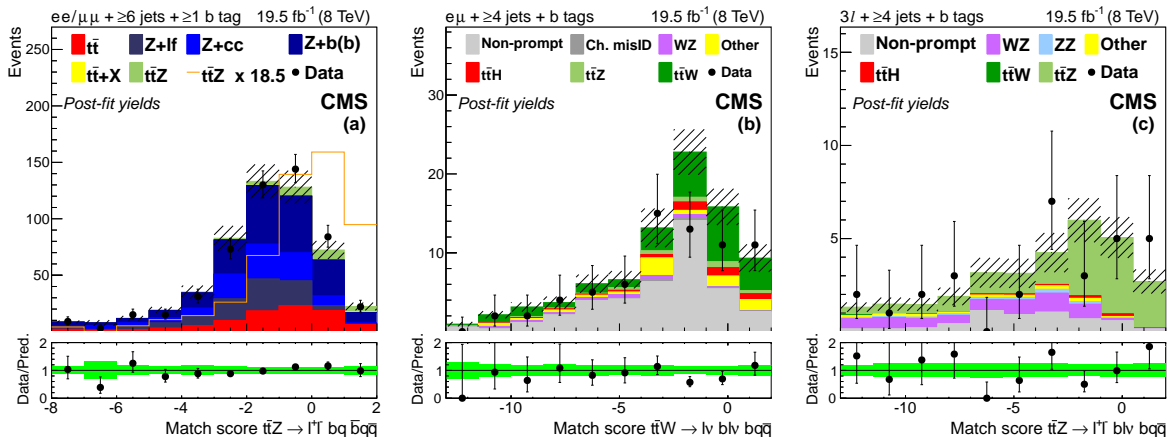


Figure 3: Distributions for match scores with signal and background yields from the final fit described in Section 10. Plot (a) shows the match score for partially reconstructed hadronic $t\bar{t}$ systems in SF OS dilepton events with six or more jets. Plots (b) and (c) show scores for fully reconstructed semileptonic $t\bar{t}$ systems in events with at least four jets, and a $SS e\mu$ pair, or three leptons, respectively. The 68% CL uncertainty in the signal plus background prediction is represented by hash marks in the stack histogram, and a green shaded region in the data-to-prediction ratio plot. The orange line in plot (a) shows the shape of the $t\bar{t}Z$ signal, suitably normalized. “Ch. misID” indicates the charge-misidentified background. “Other” backgrounds include $t\bar{t}\gamma$, $t\bar{t}\gamma^*$, $t\bar{t}WW$, $t\bar{t}Z$, WWW , WWZ , and $W^\pm W^\pm$.

8 Signal extraction

The match scores and other event reconstruction variables are combined with kinematic quantities (e.g. lepton p_T and jet CSV values) in boosted decision trees (BDTs) [35] to distinguish signal events from background processes. The linear discriminant for event reconstruction combines a large number of variables into maximally distinctive observables, achieving better separation than a BDT alone would, since fewer variables can be used in a BDT when the number of simulated events for training is limited. A separate BDT is trained for each jet category in each analysis channel, for a total of 10 BDTs. The input variables to these BDTs are described below, and listed in Appendix B, Tables 11–15.

An initial BDT in the OS channel is trained with $t\bar{t}Z$ events against the $t\bar{t}$ background, using the Z boson mass and p_T , and ΔR separation between leptons as inputs, as well as H_T^{miss} , the number of jets with $p_T > 40$ GeV, and the ratio of the M_T to the mass of a four-momentum vector composed of all the jets in the event. Event reconstruction variables include match scores to leptonic and fully hadronic $t\bar{t}$ decays, and the CSV values of jets matched to b quarks from the leptonic $t\bar{t}$ decay. The final BDT is then trained against Z boson and $t\bar{t}$ events, using the $t\bar{t}Z$ vs. $t\bar{t}$ BDT as an input, along with the two highest jet CSV values, the fifth-highest jet p_T , the number of jets with $p_T > 40$ GeV, and the ratio of the M_T to the mass of all the selected leptons and jets. Match scores to the partial five-jet and full six-jet hadronic $t\bar{t}$ system are also included, along with the minimum χ^2 value of a fit to the full hadronic $t\bar{t}$ system that uses only the W boson and top quark masses as inputs.

The SS channel BDT is trained with $t\bar{t}W$ events against $t\bar{t}$ simulation, using the lepton p_T values, p_T^{miss} , the second-highest jet CSV value, and the M_T of the system formed by the leptons, jets, and \vec{p}_T^{miss} . Event reconstruction variables include match scores to three- and four-jet $t\bar{t}W$ decays and three-jet $t\bar{t}$ decays, the matched top quark candidate mass from two jets from the W boson and the non-prompt lepton from the b -hadron decay, and the other top quark candidate M_T

from the prompt lepton, \vec{p}_T^{miss} , and the b jet in $t\bar{t}$ decays.

The BDT for the 3ℓ $t\bar{t}W$ channel is trained against $t\bar{t}$ simulation, using the p_T of the SS leptons, the highest jet p_T , the second-highest jet CSV value, p_T^{miss} , and the M_T of the leptons, jets, and \vec{p}_T^{miss} . Match scores for the two-jet $t\bar{t}W$ system and one-jet $t\bar{t}$ systems, along with the invariant mass of the prompt and non-prompt leptons matched to the same top quark in a $t\bar{t}$ decay, are also used.

The 3ℓ $t\bar{t}Z$ BDT is trained against simulated WZ and $t\bar{t}$ events, which contribute equally to the background in this channel. The input kinematic variables are the reconstructed Z boson mass (which discriminates against $t\bar{t}$), the M_T of the \vec{p}_T^{miss} , leptons and jets, and the number of medium b-tagged jets. In the three-jet category, match scores for $t\bar{t}Z$ reconstructions with one or two jets missing from the semileptonic $t\bar{t}$ decay are used as inputs; in the four jet category, match scores for three-jet systems and the full four-jet system are used.

The 4ℓ channel has too few signal and background events to train a BDT; here the number of medium b-tagged jets is used as a discriminant instead. This variable effectively separates $t\bar{t}Z$ events from the dominant ZZ background, and from subdominant non-prompt WZ, Z boson, and $t\bar{t}$ backgrounds.

The expected and observed distributions of the BDT output for each channel and category are shown in Figs. 5–6. The expected signal and background distributions represent the best fit to the data of the SM predicted backgrounds and signal, where the signal cross section is allowed to float freely. The 68% CL uncertainty in the fitted signal plus background is represented by hash marks in the stack histogram, and a green shaded region in the data-to-prediction ratio plot. The 95% CL band from the fit is shown in yellow.

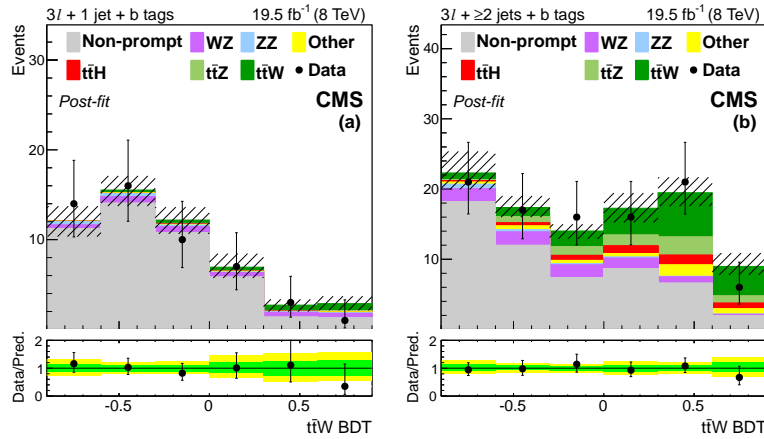


Figure 4: The final discriminant for 3ℓ $t\bar{t}W$ channel events with 1 jet (a) and ≥ 2 jets (b) after the final fit described in Section 10. The 68% CL uncertainty in the fitted signal plus background is represented by hash marks in the stack histogram, and a green shaded region in the data-to-prediction ratio plot. The 95% CL band from the fit is shown in yellow. “Other” backgrounds include $t\bar{t}\gamma$, $t\bar{t}\gamma^*$, $t\bar{t}WW$, $b\bar{t}Z$, WWW , and WWZ .

Events in the 3ℓ $t\bar{t}Z$ channel with high BDT values (>0.3 for three jet events, > -0.2 for events with four or more jets) should provide a high-purity sample of $t\bar{t}Z$ events. Data distributions of the reconstructed Z boson and top quark properties are consistent with the SM $t\bar{t}Z$ signal, as shown in Fig. 7.

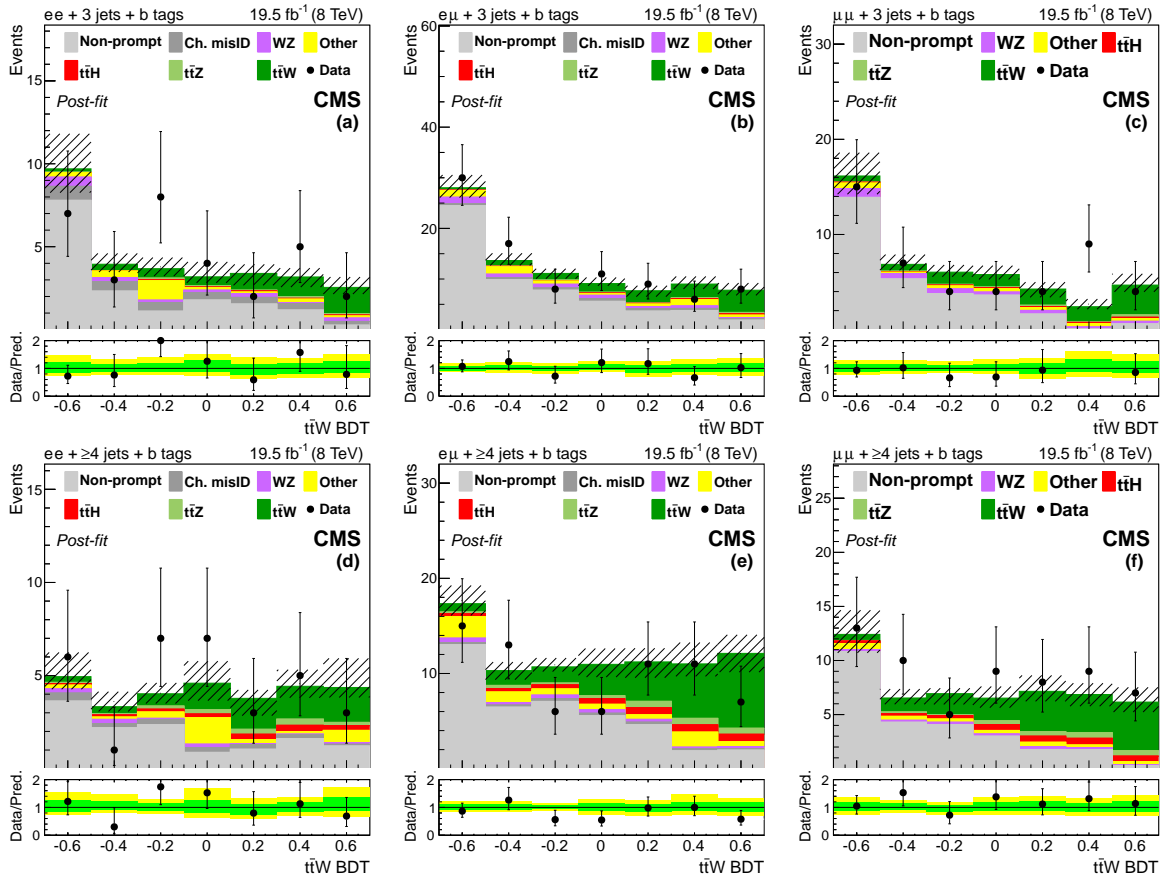


Figure 5: The final discriminant for SS $t\bar{t}W$ channel events with 3 jets (top) and ≥ 4 jets (bottom), after the final fit described in Section 10. The lepton flavors are ee (a, d), $e\mu$ (b, e), and $\mu\mu$ (c, f). The 68% CL uncertainty in the fitted signal plus background is represented by hash marks in the stack histogram, and a green shaded region in the data-to-prediction ratio plot. The 95% CL band from the fit is shown in yellow. “Ch. misID” indicates the charge-misidentified background. “Other” backgrounds include $t\bar{t}\gamma$, $t\bar{t}\gamma^*$, $t\bar{t}WW$, $t\bar{t}Z$, WWW , WWZ , and $W^\pm W^\pm$.

9 Systematic uncertainties

There are several systematic uncertainties that affect the expected rates for signal and background processes, the shape of input variables to the BDTs, or both. The most important uncertainties are on the b tagging efficiency, signal modeling, and the rates of non-prompt backgrounds and prompt processes with extra jets.

Some uncertainties affect the simulation in all of the channels, and are correlated across the entire analysis. The integrated luminosity has an uncertainty of 2.6% [9]. The total inelastic proton-proton cross section is varied up and down by 5%, which affects the number of pileup vertices, and is propagated to the output distributions [36].

The properties and reconstruction efficiencies of different objects have their own uncertainties. The uncertainty in the jet energy scale [26] is accounted for by shifting the energy scale up and down by one standard deviation for all simulated processes, and evaluating the output distributions with the shifted energy scale. The shape of the CSV distribution for light flavor or gluon jets, c jets, and b jets has uncertainties associated with the method used to match the CSV shapes in data and simulation, as detailed in Ref. [27]. Calibration regions for light flavor jets have some contamination from heavy flavor jets, and vice versa. The associated uncertainty

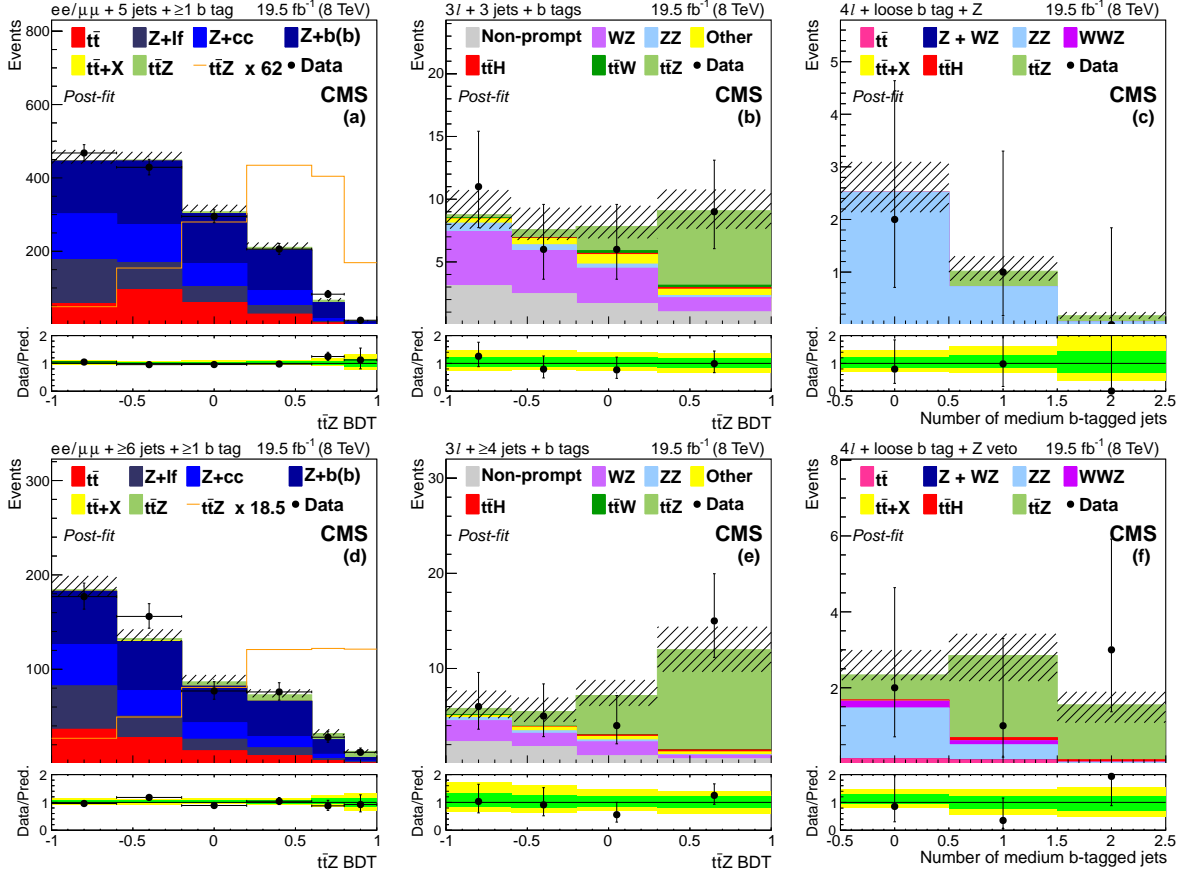


Figure 6: The final discriminant for $\bar{t}\bar{t}Z$ channel events with two OS leptons and 5 jets (a) or ≥ 6 jets (d), three leptons and 3 jets (b) or ≥ 4 jets (e), or four leptons and two lepton pairs (c) or exactly one lepton pair (f) consistent with a $Z \rightarrow \ell\ell$ decay, after the final fit described in Section 10. The 68% CL uncertainty in the fitted signal plus background is represented by hash marks in the stack histogram, and a green shaded region in the data-to-prediction ratio plot. The 95% CL band from the fit is shown in yellow. The orange line shows the shape of the $\bar{t}\bar{t}Z$ signal, suitably normalized. The $\bar{t}\bar{t}+X$ background includes $\bar{t}\bar{t}W$, $\bar{t}\bar{t}H$, and $\bar{t}\bar{t}WW$; “Other” backgrounds include $\bar{t}\bar{t}\gamma$, $\bar{t}\bar{t}\gamma^*$, $\bar{t}\bar{t}WW$, $t\bar{b}Z$, WWW , and WWZ .

in the final light or heavy flavor CSV shape is accounted for by varying the expected yields of contaminating jets up and down by one standard deviation, and propagating the result to the final CSV distribution. The weights for these alternate shapes are applied to produce alternate final discriminant histograms in each channel. Likewise there are uncertainties from the limited number of events in the calibration regions; these are assessed using the maximum linear and quadratic deformations of the CSV shape within an envelope whose size is determined by the magnitude of the statistical uncertainty. Because there is no calibration region to determine the CSV shape of c jets in data, they receive no correction factors, but have all the b jet uncertainties applied to them, multiplied by a factor of two so that they include the scale factor values for b jets.

Prompt electron and muon efficiency uncertainties are computed using high-purity dilepton samples in data from Z boson decays. These include rate uncertainties associated with the trigger efficiency, reconstruction efficiency, and the fraction of prompt leptons passing the tight, loose, and charge ID selection criteria.

The rate of non-prompt leptons passing the tight lepton selection receives a 40% uncertainty

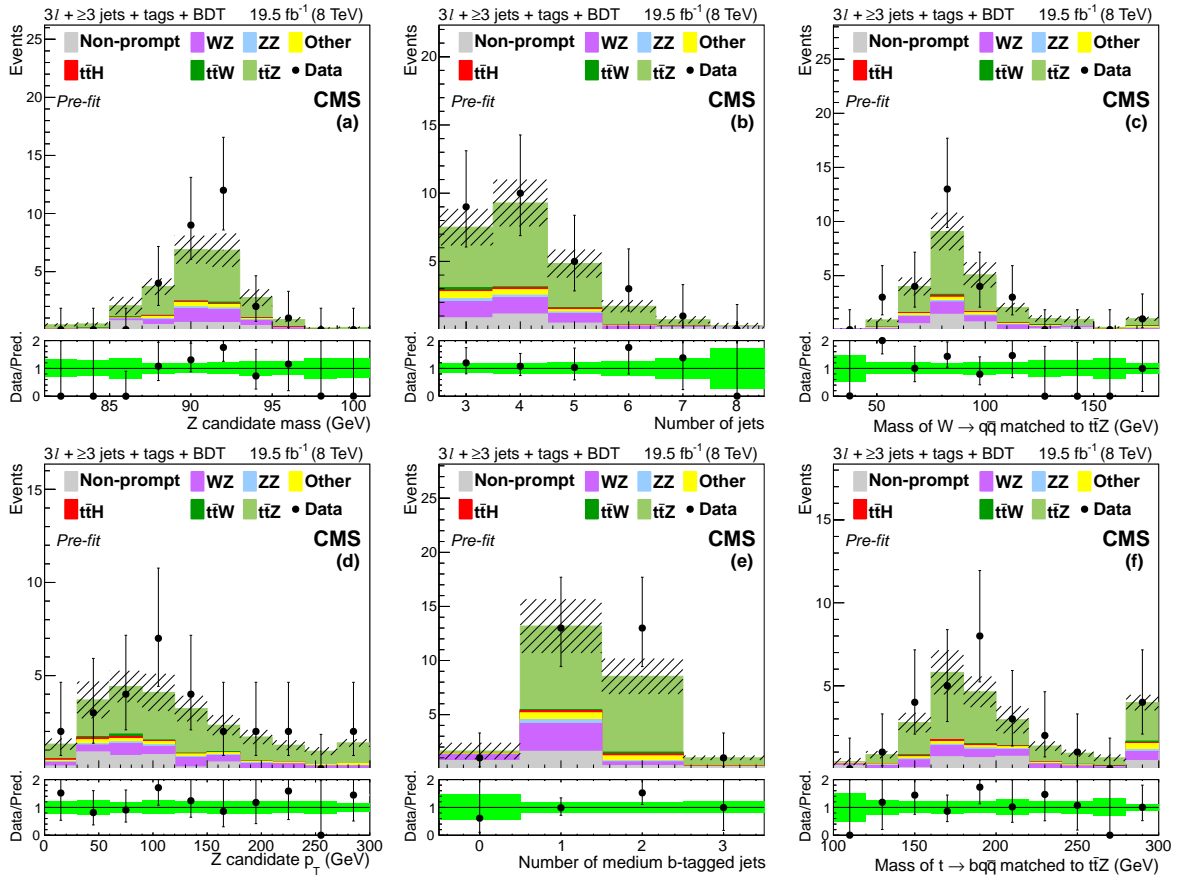


Figure 7: Distributions of the mass (a) and p_T (d) of the lepton pair identified with the Z boson decay, the number of jets (b) and medium b-tagged jets (e), and the mass of the best fit dijet pair from a W boson decay (c) and trijet system from a top quark decay (f). The plots show signal-like events from the 3ℓ $t\bar{t}Z$ channel (3 jets with $\text{BDT} > 0.3$ and ≥ 4 jets with $\text{BDT} > -0.2$) before the final fit described in Section 10 is performed. The green band in the data-to-prediction ratio plot denotes the 68% CL rate and shape uncertainties in the signal plus background prediction. “Other” backgrounds include $t\bar{t}\gamma$, $t\bar{t}\gamma^*$, $t\bar{t}WW$, $t\bar{t}Z$, WWW , and WWZ .

for electrons and a 60% uncertainty for muons, based on the agreement between expected and observed yields in control regions in data, as described in Section 6. Additional uncertainties of 50% and 100% are assessed on the rates of non-prompt leptons with medium and high p_T , respectively, because of the limited number of events in the sample used to find the misidentification rates. These uncertainties are applied separately for electrons and muons, and are uncorrelated between the SS and 3ℓ channels, to account for possible differences in the sources of non-prompt leptons. While the uncertainties on event yields with non-prompt electrons and muons are initially large, the final fit constrains them to 10–15% using bins in the final discriminants which contain mostly non-prompt backgrounds.

The rates of charge misidentified electrons in the SS channels receive a 30% rate uncertainty, based on the agreement between predicted and observed SS dielectron events consistent with a Z boson decay.

Theoretical uncertainties from the PDFs of different simulated processes, as well as the choice of renormalization and factorization scales, are accounted for with rate uncertainties in all signal and backgrounds processes. The rate uncertainties for $t\bar{t}W$ and $t\bar{t}Z$ are 10% and 11%, respectively, from the choice of scales [1], and 7.2% and 8.2% from the PDFs [37, 38]. In addition, shape

uncertainties derived from simulation generated with different PDF sets and PYTHIA tunes are applied to the $t\bar{t}W$, $t\bar{t}Z$, and $t\bar{t}H$ processes using linear and quadratic deformations of 10–11% on the final discriminant shape. The $t\bar{t}W$ and $t\bar{t}Z$ rate uncertainties are not included in the $t\bar{t}W$ and $t\bar{t}Z$ cross section measurements, respectively, and neither is used in the simultaneous measurement of the $t\bar{t}W$ and $t\bar{t}Z$ cross sections.

The systematic uncertainty in top quark p_T reweighting in simulated $t\bar{t}$ events is assessed by applying no top quark p_T weight for the lower systematic uncertainty, and twice the weight for the upper systematic uncertainty. Since neither higher-order theoretical calculations [39] nor independent control region studies currently constrain the normalization of the $t\bar{t}+c\bar{c}$, $t\bar{t}+b$, or $t\bar{t}+b\bar{b}$ processes to better than 50% accuracy, an extra 50% uncorrelated rate uncertainty is assigned to each process. An additional shape uncertainty is applied to the ratio of the M_T to the invariant mass of the system of jets in $t\bar{t}$ events with five, or six or more jets.

Because the Z boson, WZ, and ZZ simulations are used to model events with more jets than there are extra partons in the generated event, rate uncertainties are assigned to these processes. Events with a Z boson plus five jets and six or more jets receive uncorrelated 30% rate uncertainties, based on the extrapolation from Z boson events with four jets and no medium b-tagged jets to those with at least one medium b tag. Diboson WZ and ZZ events with three jets and four or more jets have uncorrelated 40% and 60% uncertainties, respectively, due to the limited number of events in the light flavor sideband used to calibrate jet multiplicity. Diboson events with extra heavy flavor jets receive uncertainties identical to the $t\bar{t}$ plus heavy flavor simulation. The good data-to-simulation agreement in dileptonic Z boson events with four jets and one or two medium b tags constrains the $Z + c\bar{c}$, $Z + b$, and $Z + b\bar{b}$ uncertainties to 30% each. Simulated Z boson events have extra shape uncertainties in H_T^{miss} and the M_T -to-mass ratio of jets, uncorrelated between events with five and six or more jets, and between the different jet flavor subsamples. These account for possible data-to-simulation differences seen in Z boson events with four or more jets (excluding the $t\bar{t}Z$ signal region). Although these uncertainties are large, the Z boson and diboson backgrounds are well separated from the $t\bar{t}Z$ signal using the final discriminants, so they have a small effect on the final measurement.

Rare processes with low expected yields such as triboson production (WWW, WWZ), associated production of a Z boson with a single top quark (tbZ), and $t\bar{t}$ with an on-shell or off-shell photon ($t\bar{t}\gamma/t\bar{t}\gamma^*$) or two W bosons ($t\bar{t}WW$) get 50% rate uncertainties, because they are either calculated at leading order or require extra jets or b jets to enter the signal region.

The expected impact of different sources of systematic uncertainty is estimated by removing groups of uncertainties one at a time and gauging the improvement in the signal strength precision, as measured using pseudo-data from simulation. (The measurement technique is described in the next section.) If we expect to measure a signal strength of $1 \pm \delta_i$ with all the systematic uncertainties included, and expect to measure $1 \pm \delta_{i \neq j}$ with fewer uncertainties, a large reduction in uncertainty $\epsilon_j = \delta_i - \delta_{i \neq j}$ indicates that the removed uncertainties have a significant impact on the measurement. Uncertainties in b tagging efficiency, signal modeling, and rates of prompt processes with extra jets are found to have the greatest effect on the $t\bar{t}Z$ signal precision, while the $t\bar{t}W$ measurement is most impacted by uncertainties in the non-prompt backgrounds, b tagging efficiency, and signal modeling. The full set of systematic uncertainties and their expected effects are shown in Table 6. Because we are measuring ϵ_j and not δ_j , we do not expect the quantities in Table 6 to add in quadrature.

Table 6: Reduction in the expected signal strength uncertainties produced by removing sets of systematic uncertainties. The quantities in each column are not expected to add in quadrature.

Systematic uncertainties removed	$t\bar{t}W$	$t\bar{t}Z$
Signal modeling	5.2%	7.1%
Non-prompt backgrounds	12.5%	0.5%
Inclusive prompt backgrounds	0.7%	2.6%
Prompt backgrounds with extra jets	0.2%	3.4%
Prompt backgrounds with extra heavy flavor jets	<0.1%	1.1%
b tagging efficiency	6.1%	7.3%
Jet energy scale	1.4%	<0.1%
Lepton ID and trigger efficiency	0.3%	0.5%
Integrated luminosity and pileup	0.7%	0.5%
Bin-by-bin statistical uncertainty in the prediction	4.4%	1.2%
All systematic uncertainties removed	31%	29%

10 Cross section measurement

The statistical procedure used to compute the $t\bar{t}W$ and $t\bar{t}Z$ cross sections and their corresponding significances is the same as the one used for the LHC Higgs boson analyses, and is described in detail in Refs. [40, 41]. A binned likelihood function $L(\mu, \theta)$ is constructed, which is the product of Poisson probabilities for all bins in the final discriminants of every channel. The signal strength parameter μ characterizes the amount of signal, with $\mu = 1$ corresponding to the SM signal hypothesis, and $\mu = 0$ corresponding to the background-only hypothesis. Systematic uncertainties in the signal and background predictions are represented by a set of nuisance parameters, denoted θ . Each nuisance parameter represents a different source of uncertainty. When multiple channels have the same source of uncertainty, the nuisance parameter is correlated across the channels, allowing certain initially large systematic uncertainties (such as the rate of non-prompt leptons passing the tight selection) to be constrained in bins with a large number of data events but few expected signal events.

To test how consistent the data are with a hypothesized value of μ , we consider the profile likelihood ratio test statistic $q(\mu) = -2 \ln L(\mu, \hat{\theta}_\mu) / L(\hat{\mu}, \hat{\theta})$, where $\hat{\theta}_\mu$ denotes the set of values of the nuisance parameters θ that maximizes the likelihood L for the given μ . The denominator is the likelihood maximized over all μ and θ . This test statistic is integrated using asymptotic formulae [42] to obtain the p -value, i.e. the probability under the signal-plus-background hypothesis of finding data of equal or greater incompatibility with the background-only hypothesis. Results are reported both in terms of the best fit cross section and μ values and their associated uncertainties, and in terms of the significance of observation of the two signal processes.

We perform separate one-dimensional fits for the $t\bar{t}W$ and $t\bar{t}Z$ cross sections using the relevant channels for each process. The fit for each cross section is performed with the other cross section set to the SM value with the uncertainty coming from theory calculations. The resulting measurements and significances are reported in Tables 7 and 8. The $t\bar{t}Z$ cross section is measured with a precision of 25%, and agrees well with the SM prediction. The observed $t\bar{t}W$ cross section is higher than expected, driven by an excess of signal-like SS dimuon events in the data. Most of the signal-like dimuon events with four or more jets also contributed to a similar excess seen in the CMS $t\bar{t}H$ search [27]. In both analyses, a close examination yielded no evidence of mismodeling or underestimated backgrounds, and the excess events appear consistent with a $t\bar{t}W$ or $t\bar{t}H$ signal. The best fit values for the $t\bar{t}W$ and $t\bar{t}Z$ cross sections are compatible with the SM expectation at the 13% and 60% CL, respectively. Taking into account significant differences

in event selection, this result is also consistent with the previous CMS measurement [3], which it supersedes.

We also perform a simultaneous fit of both processes using all the channels. Figure 8 shows the two-dimensional likelihood scan over $\sigma(\text{t}\bar{\text{t}}\text{W})$ and $\sigma(\text{t}\bar{\text{t}}\text{Z})$. The respective best fit values are found to be 350_{-123}^{+150} fb and 245_{-80}^{+104} fb, compatible at the 15% CL with the SM expectation [1, 43].

Table 7: Expected and observed measurements of the cross section and signal strength with 68% CL ranges and significances for $\text{t}\bar{\text{t}}\text{W}$, in SS dilepton and 3ℓ channels.

Channels	Cross section (fb)		Signal strength (μ)		Significance (σ)	
	Expected	Observed	Expected	Observed	Expected	Observed
SS	203_{-73}^{+88}	414_{-112}^{+135}	$1.00_{-0.36}^{+0.45}$	$2.04_{-0.61}^{+0.74}$	3.4	4.9
3ℓ	203_{-194}^{+215}	210_{-203}^{+225}	$1.00_{-0.96}^{+1.09}$	$1.03_{-0.99}^{+1.07}$	1.0	1.0
SS + 3ℓ	203_{-71}^{+84}	382_{-102}^{+117}	$1.00_{-0.35}^{+0.43}$	$1.88_{-0.56}^{+0.66}$	3.5	4.8

Table 8: Expected and observed measurements of the cross section and signal strength with 68% CL ranges and significances for $\text{t}\bar{\text{t}}\text{Z}$, in OS dilepton, 3ℓ , and 4ℓ channels.

Channels	Cross section (fb)		Signal strength (μ)		Significance (σ)	
	Expected	Observed	Expected	Observed	Expected	Observed
OS	206_{-118}^{+142}	257_{-129}^{+158}	$1.00_{-0.57}^{+0.72}$	$1.25_{-0.62}^{+0.76}$	1.8	2.1
3ℓ	206_{-63}^{+79}	257_{-67}^{+85}	$1.00_{-0.32}^{+0.42}$	$1.25_{-0.36}^{+0.45}$	4.6	5.1
4ℓ	206_{-109}^{+153}	228_{-107}^{+150}	$1.00_{-0.53}^{+0.77}$	$1.11_{-0.52}^{+0.76}$	2.7	3.4
OS + 3ℓ + 4ℓ	206_{-52}^{+62}	242_{-55}^{+65}	$1.00_{-0.27}^{+0.34}$	$1.18_{-0.29}^{+0.35}$	5.7	6.4

11 Extended interpretation

Direct measurement of the $\text{t}\bar{\text{t}}\text{Z}$ and $\text{t}\bar{\text{t}}\text{W}$ cross sections can be applied to searches for new physics (NP) within the framework of an effective field theory. The effects of new particles or interactions can be captured in a model-independent way by supplementing the SM Lagrangian with higher-dimensional operators involving SM fields. The effective Lagrangian can be written [44] as an expansion in the inverse of the cutoff energy scale, $1/\Lambda$:

$$\begin{aligned}
\mathcal{L}_{\text{eff}} &= \mathcal{L}_{\text{SM}} + \frac{1}{\Lambda} \mathcal{L}_1 + \frac{1}{\Lambda^2} \mathcal{L}_2 + \dots \\
&= \mathcal{L}_{\text{SM}} + \frac{1}{\Lambda} \sum_i (c_i \mathcal{O}_i + \text{h.c.}) + \frac{1}{\Lambda^2} \sum_j (c_j \mathcal{O}_j + \text{h.c.}) + \dots,
\end{aligned} \tag{1}$$

where \mathcal{L}_{SM} is the SM Lagrangian density of dimension four, \mathcal{L}_1 is of dimension five, etc. The Wilson coefficients c_i and c_j are numerical constants that parameterize the strength of the non-standard interactions, and \mathcal{O}_i and \mathcal{O}_j are operators corresponding to combinations of SM fields. Hermitian conjugate terms are denoted h.c. Good agreement between data and SM expectations suggests that deviations due to NP are small and it is reasonable to work in the first order of c_i and c_j [45]; we limit ourselves to this domain.

It is not possible to construct a dimension-five operator that conserves lepton number [44], so only dimension-six operators are considered in this work. Assuming baryon number con-

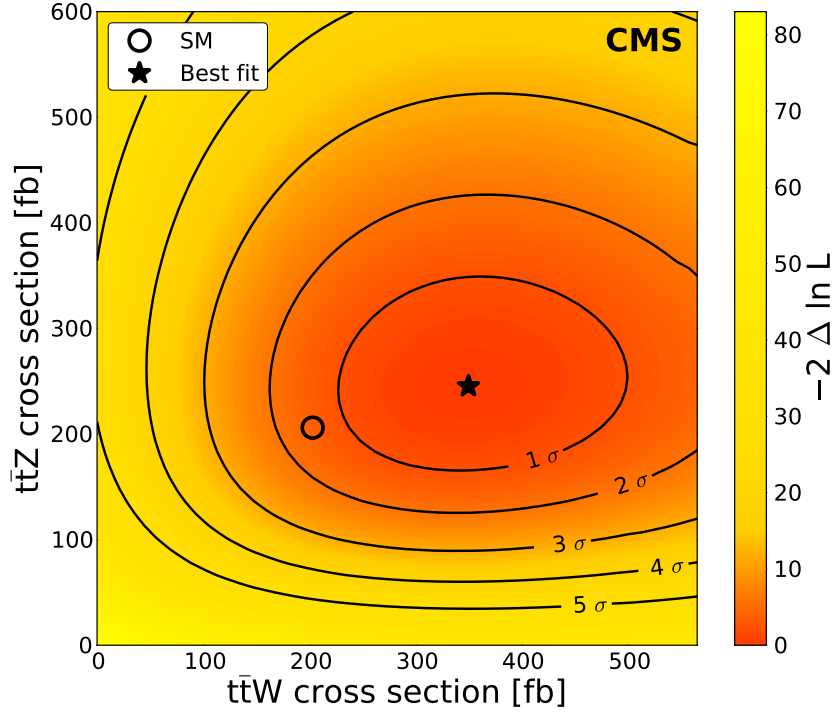


Figure 8: Profile likelihood as a function of $\sigma(\bar{t}tW)$ and $\sigma(\bar{t}tZ)$. Lines denote the 1 to 5 standard deviation (σ) CL contours.

servation, there are 59 independent dimension-six operators [46]. We follow the notation and operator naming scheme introduced in Ref. [47]. We study the effect of these operators on the tZ coupling constants and the ttW and ttZ cross sections, and compare them to the measured values.

11.1 Constraints on the axial and vector components of the tZ coupling

Indirect measurements of the top quark to Z boson coupling include, for example, precision studies of the $Z \rightarrow b\bar{b}$ branching fraction at LEP and the SLC [48–53]. The ttZ process provides the first experimentally accessible direct probe of the tZ coupling.

The SM ttZ interaction Lagrangian can be written in terms of the vector and axial couplings C_V^{SM} and C_A^{SM} , which can be precisely calculated. In the effective field theory approach, the modified couplings $C_{1,V}$ and $C_{1,A}$ are considered, which can be written in terms of the SM contribution plus deviations due to the Wilson coefficients c_j of dimension-six operators [54], scaled by Λ , the Higgs field vacuum expectation value v , and the weak mixing angle θ_w :

$$\begin{aligned}
 C_{1,V} &= C_V^{\text{SM}} + \frac{1}{4 \sin \theta_w \cos \theta_w} \frac{v^2}{\Lambda^2} \text{Re}[\bar{c}'_{HQ} - \bar{c}_{HQ} - \bar{c}_{Hu}], \\
 C_{1,A} &= C_A^{\text{SM}} - \frac{1}{4 \sin \theta_w \cos \theta_w} \frac{v^2}{\Lambda^2} \text{Re}[\bar{c}'_{HQ} - \bar{c}_{HQ} + \bar{c}_{Hu}].
 \end{aligned}
 \tag{2}$$

A method for calculating $\sigma(\bar{t}tZ)$ in terms of $C_{1,V}$ and $C_{1,A}$ has been presented in Ref. [54]. The cross section depends on a constant term, linear and quadratic terms in $C_{1,V}$ and $C_{1,A}$, and a mixed term. Each of these six terms is scaled by a factor which was evaluated in Ref. [54]

by calculating the 7 TeV cross section at six points and solving the system of equations. To extrapolate to 8 TeV, we scale $\sigma(\bar{t}tZ)(C_{1,V}, C_{1,A})$ linearly by the ratio of the theoretical $\bar{t}tZ$ cross sections at 7 and 8 TeV. From this we define the signal strength parameter $\mu_{\bar{t}tZ}$ in terms of $C_{1,V}$ and $C_{1,A}$, and a profile likelihood ratio test statistic, as described in Section 10. We perform a two-dimensional scan of the $(C_{1,V}, C_{1,A})$ phase space to extract the best fit values, which are found to satisfy the constraint:

$$74.6 + 0.5 C_{1,V} + 189.4 C_{1,V}^2 - 16.3 C_{1,A} + 359.7 C_{1,A}^2 = 242. \quad (3)$$

The difference between the profile likelihood and the best fit profile likelihood is plotted as a function of the relative vector and axial components $\Delta C_{1,V} = C_{1,V}/C_V^{\text{SM}} - 1$ and $\Delta C_{1,A} = C_{1,A}/C_A^{\text{SM}} - 1$ in Fig. 9.

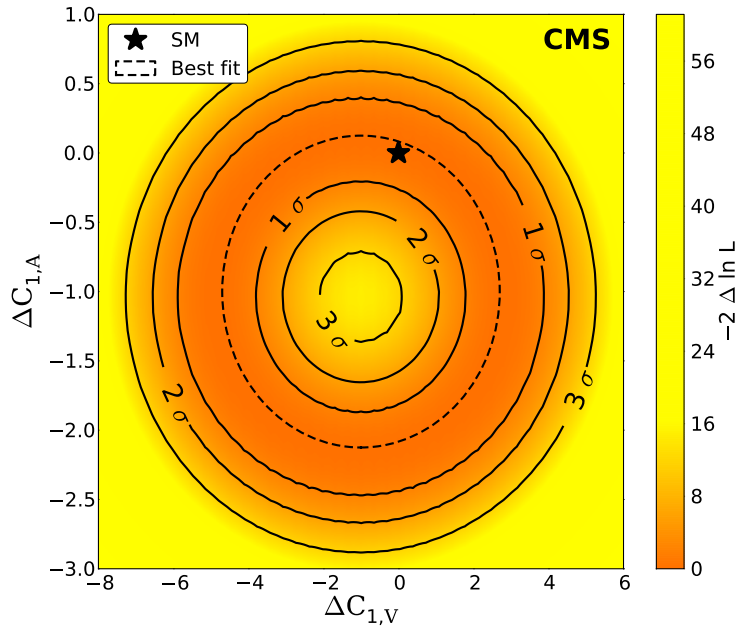


Figure 9: Difference between the profile likelihood and the best fit profile likelihood functions for the relative vector and axial components of the tZ coupling. Contours corresponding to the best fit and the 1, 2, and 3 standard deviation (σ) CLs are shown in lines.

11.2 Constraints on dimension-six operators

Both indirect and direct constraints on dimension-six operators are documented in Refs. [45, 54–59]. To study the effects of NP on the $\bar{t}tW$ and $\bar{t}tZ$ processes, we use the FEYNRULES [60] implementation from Ref. [47]. This implementation is used with MADGRAPH 5 [10] to compute cross sections as a function of $(v^2/\Lambda^2)c_j$, henceforward simply denoted by c_j . Cross sections were computed for the production of $\bar{t}t$, a Higgs boson, $\bar{t}tZ$, and $\bar{t}tW$, sampling 20 points for each c_j . For each sampled point, all $c_{k \neq j}$ were fixed at zero. From this survey, we select five operators as of particular interest because they have a small effect on inclusive Higgs boson and $\bar{t}t$ production, and a large effect on $\bar{t}tZ$, $\bar{t}tW$, or both: \bar{c}_{uB} , \bar{c}'_{HQ} , \bar{c}_{HQ} , \bar{c}_{Hu} , and \bar{c}_{3W} . An alternative way to display the effect of each c_j is shown in Fig. 10, where sampled values are plotted in the $(\sigma(\bar{t}tW), \sigma(\bar{t}tZ))$ plane. From these it is clear that \bar{c}_{uB} , \bar{c}_{Hu} , and \bar{c}_{HQ} affect only $\bar{t}tZ$, whereas \bar{c}_{3W} only affects $\bar{t}tW$, and \bar{c}'_{HQ} affects both processes. For each of the five operators, we perform a finer scan of 200 cross section points and use a spline fit to obtain an expression

for the cross section in terms of c_j , $\sigma(\bar{t}\bar{t}Z)_{\text{SM+NP}}(c_j)$. We define the signal strength $\mu_{\bar{t}\bar{t}Z}(c_j)$ to be the ratio of the $\bar{t}\bar{t}Z$ production cross section to the combined expectations from SM and NP $\sigma(\bar{t}\bar{t}Z)_{\text{SM+NP}}(c_j)$, and likewise for $\bar{t}\bar{t}W$. From this we can define a profile likelihood ratio in terms of c_j , similarly to what is described in Section 10.

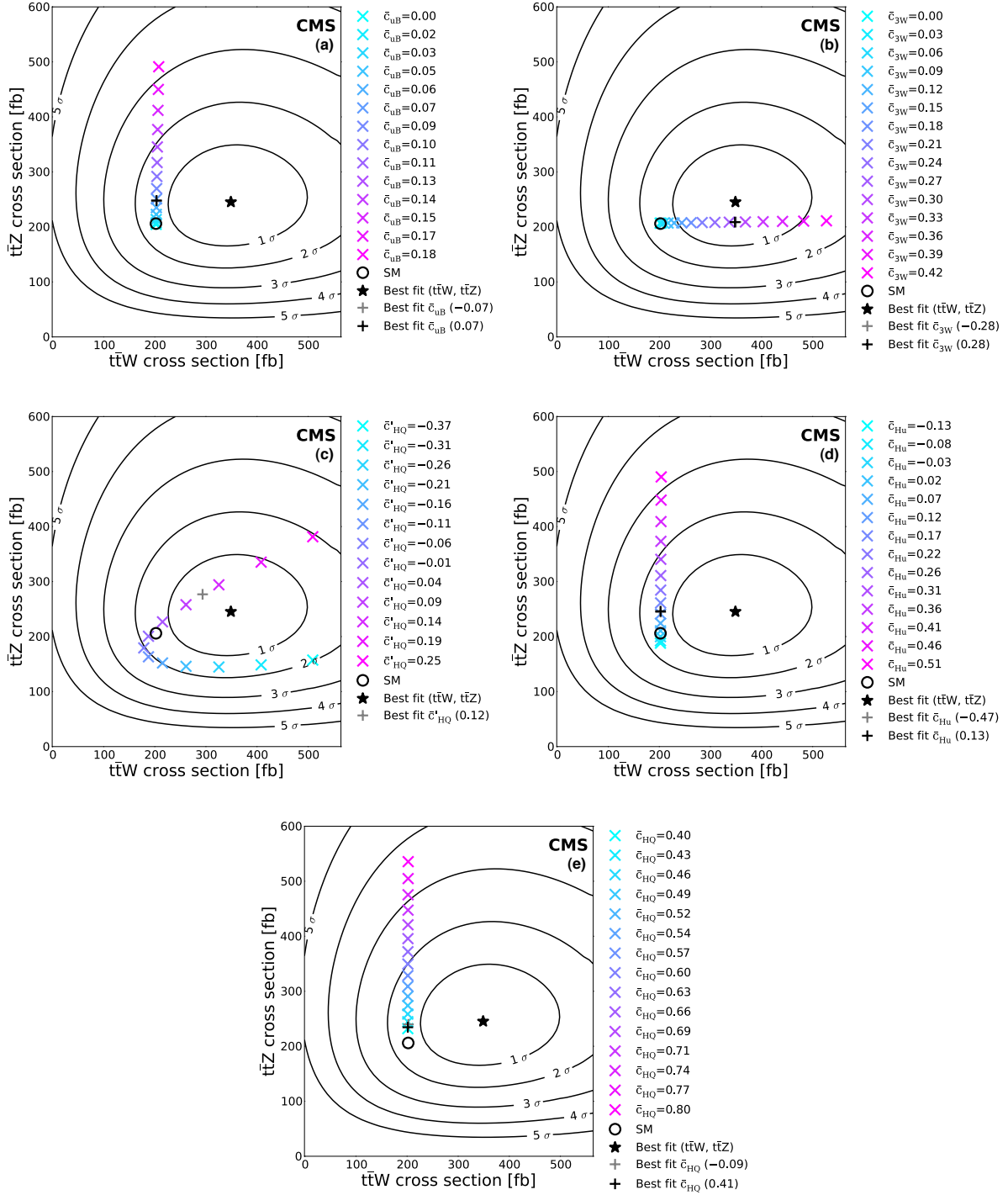


Figure 10: Sampled coefficient values for \bar{c}_{ub} (a), \bar{c}_{3W} (b), \bar{c}'_{HQ} (c), \bar{c}_{Hu} (d), and \bar{c}_{HQ} (e), plotted in the $(\sigma(\bar{t}\bar{t}W), \sigma(\bar{t}\bar{t}Z))$ plane. There are typically two best fit values, one greater and one less than zero, which lie on top of one another in the plane.

Best fit values, along with 1σ and 2σ CL ranges are summarized in Table 9. Operators that affect either the $t\bar{t}W$ or the $t\bar{t}Z$ cross section, but not both, have symmetric likelihood distributions and thus have two best fit values. Bounds on \bar{c}'_{HQ} , \bar{c}_{HQ} , and \bar{c}_{Hu} are stricter than those derived in Ref. [54] from CMS and ATLAS searches for $t\bar{t}Z$ using LHC data at 7 TeV. Constraints on \bar{c}_{uB} are tighter than those derived in Ref. [59].

Table 9: Constraints from this $t\bar{t}Z$ and $t\bar{t}W$ measurement on selected dimension-six operators.

Operator	Best fit point(s)	1 standard deviation CL	2 standard deviation CL
\bar{c}_{uB}	-0.07 and 0.07	[-0.11, 0.11]	[-0.14, 0.14]
\bar{c}_{3W}	-0.28 and 0.28	[-0.36, -0.18] and [0.18, 0.36]	[-0.43, 0.43]
\bar{c}'_{HQ}	0.12	[-0.07, 0.18]	[-0.33, -0.24] and [-0.02, 0.23]
\bar{c}_{Hu}	-0.47 and 0.13	[-0.60, -0.23] and [-0.11, 0.26]	[-0.71, 0.37]
\bar{c}_{HQ}	-0.09 and 0.41	[-0.22, 0.08] and [0.24, 0.54]	[-0.31, 0.63]

12 Summary

An observation of top quark pairs produced in association with a Z boson and measurements of the $t\bar{t}W$ and $t\bar{t}Z$ cross sections have been made, using 19.5 fb^{-1} of 8 TeV pp collision data collected by the CMS detector at the LHC. Signatures from different decay modes of the top quark pair resulting in final states with two, three, and four leptons have been analyzed. Signal events have been identified by uniquely matching reconstructed leptons and jets to final state particles from $t\bar{t}W$ and $t\bar{t}Z$ decays. Results from two independent $t\bar{t}W$ channels and three $t\bar{t}Z$ channels have been presented, along with combined measurements. The combined $t\bar{t}W$ cross section measurement in same-sign dilepton and three-lepton events is $382^{+117}_{-102} \text{ fb}$, 4.8 standard deviations from the background-only hypothesis, where a significance of 3.5 standard deviations is expected in the standard model. Combining opposite-sign dilepton, three-lepton, and four-lepton channels, the $t\bar{t}Z$ cross section is measured to be $242^{+65}_{-55} \text{ fb}$, an observation with a significance of 6.4 standard deviations from the background-only hypothesis, and in agreement with the standard model expectation. Using the measured cross sections, limits have been placed on the vector and axial couplings of the Z boson to the top quark, and on the Wilson coefficients of five dimension-six operators parameterizing new physics: \bar{c}_{uB} , \bar{c}'_{HQ} , \bar{c}_{HQ} , \bar{c}_{Hu} , and \bar{c}_{3W} . These measurements are compatible with the standard model predictions, and are the most sensitive reported to date to these high mass scale processes.

Acknowledgements

We congratulate our colleagues in the CERN accelerator departments for the excellent performance of the LHC and thank the technical and administrative staffs at CERN and at other CMS institutes for their contributions to the success of the CMS effort. In addition, we gratefully acknowledge the computing centers and personnel of the Worldwide LHC Computing Grid for delivering so effectively the computing infrastructure essential to our analyses. Finally, we acknowledge the enduring support for the construction and operation of the LHC and the CMS detector provided by the following funding agencies: the Austrian Federal Ministry of Science, Research and Economy and the Austrian Science Fund; the Belgian Fonds de la Recherche Scientifique, and Fonds voor Wetenschappelijk Onderzoek; the Brazilian Funding Agencies (CNPq, CAPES, FAPERJ, and FAPESP); the Bulgarian Ministry of Education and Science; CERN; the Chinese Academy of Sciences, Ministry of Science and Technology, and National Natural Science Foundation of China; the Colombian Funding Agency (COLCIENCIAS);

the Croatian Ministry of Science, Education and Sport, and the Croatian Science Foundation; the Research Promotion Foundation, Cyprus; the Ministry of Education and Research, Estonian Research Council via IUT23-4 and IUT23-6 and European Regional Development Fund, Estonia; the Academy of Finland, Finnish Ministry of Education and Culture, and Helsinki Institute of Physics; the Institut National de Physique Nucléaire et de Physique des Particules / CNRS, and Commissariat à l'Énergie Atomique et aux Énergies Alternatives / CEA, France; the Bundesministerium für Bildung und Forschung, Deutsche Forschungsgemeinschaft, and Helmholtz-Gemeinschaft Deutscher Forschungszentren, Germany; the General Secretariat for Research and Technology, Greece; the National Scientific Research Foundation, and National Innovation Office, Hungary; the Department of Atomic Energy and the Department of Science and Technology, India; the Institute for Studies in Theoretical Physics and Mathematics, Iran; the Science Foundation, Ireland; the Istituto Nazionale di Fisica Nucleare, Italy; the Ministry of Science, ICT and Future Planning, and National Research Foundation (NRF), Republic of Korea; the Lithuanian Academy of Sciences; the Ministry of Education, and University of Malaya (Malaysia); the Mexican Funding Agencies (CINVESTAV, CONACYT, SEP, and UASLP-FAI); the Ministry of Business, Innovation and Employment, New Zealand; the Pakistan Atomic Energy Commission; the Ministry of Science and Higher Education and the National Science Center, Poland; the Fundação para a Ciência e a Tecnologia, Portugal; JINR, Dubna; the Ministry of Education and Science of the Russian Federation, the Federal Agency of Atomic Energy of the Russian Federation, Russian Academy of Sciences, and the Russian Foundation for Basic Research; the Ministry of Education, Science and Technological Development of Serbia; the Secretaría de Estado de Investigación, Desarrollo e Innovación and Programa Consolider-Ingenio 2010, Spain; the Swiss Funding Agencies (ETH Board, ETH Zurich, PSI, SNF, UniZH, Canton Zurich, and SER); the Ministry of Science and Technology, Taipei; the Thailand Center of Excellence in Physics, the Institute for the Promotion of Teaching Science and Technology of Thailand, Special Task Force for Activating Research and the National Science and Technology Development Agency of Thailand; the Scientific and Technical Research Council of Turkey, and Turkish Atomic Energy Authority; the National Academy of Sciences of Ukraine, and State Fund for Fundamental Researches, Ukraine; the Science and Technology Facilities Council, UK; the US Department of Energy, and the US National Science Foundation.

Individuals have received support from the Marie-Curie program and the European Research Council and EPLANET (European Union); the Leventis Foundation; the A. P. Sloan Foundation; the Alexander von Humboldt Foundation; the Belgian Federal Science Policy Office; the Fonds pour la Formation à la Recherche dans l'Industrie et dans l'Agriculture (FRRIA-Belgium); the Agentschap voor Innovatie door Wetenschap en Technologie (IWT-Belgium); the Ministry of Education, Youth and Sports (MEYS) of the Czech Republic; the Council of Science and Industrial Research, India; the HOMING PLUS program of the Foundation for Polish Science, cofinanced from European Union, Regional Development Fund; the OPUS program of the National Science Center (Poland); the Compagnia di San Paolo (Torino); the Consorzio per la Fisica (Trieste); MIUR project 20108T4XTM (Italy); the Thalís and Aristeia programs cofinanced by EU-ESF and the Greek NSRF; the National Priorities Research Program by Qatar National Research Fund; the Rachadapisek Sompot Fund for Postdoctoral Fellowship, Chulalongkorn University (Thailand); and the Welch Foundation, contract C-1845.

References

- [1] M. V. Garzelli, A. Kardos, C. G. Papadopoulos, and Z. Trocsanyi, “ $t\bar{t}W^\pm$ and $t\bar{t}Z$ hadroproduction at NLO accuracy in QCD with parton shower and hadronization effects”, *JHEP* **11** (2012) 056, doi:10.1007/JHEP11(2012)056, arXiv:1208.2665.

- [2] CMS Collaboration, “Measurement of associated production of vector bosons and $t\bar{t}$ in pp collisions at $\sqrt{s} = 7$ TeV”, *Phys. Rev. Lett.* **110** (2013) 172002, doi:10.1103/PhysRevLett.110.172002, arXiv:1303.3239.
- [3] CMS Collaboration, “Measurement of top quark-antiquark pair production in association with a W or Z boson in pp collisions at $\sqrt{s} = 8$ TeV”, *Eur. Phys. J. C* **74** (2014) 3060, doi:10.1140/epjc/s10052-014-3060-7, arXiv:1406.7830.
- [4] ATLAS Collaboration, “Measurement of the $t\bar{t}W$ and $t\bar{t}Z$ production cross sections in pp collisions at $\sqrt{s} = 8$ TeV with the ATLAS detector”, (2015). arXiv:1509.05276. Submitted to *JHEP*.
- [5] Particle Data Group, “Review of particle physics”, *Chin. Phys. C* **38** (2014) 090001, doi:10.1088/1674-1137/38/9/090001.
- [6] CMS Collaboration, “Particle-Flow Event Reconstruction in CMS and Performance for Jets, Taus, and MET”, CMS Physics Analysis Summary CMS-PAS-PFT-09-001, 2009.
- [7] CMS Collaboration, “Commissioning of the particle-flow event reconstruction with the first LHC collisions recorded in the CMS detector”, CMS Physics Analysis Summary CMS-PAS-PFT-10-001, 2010.
- [8] CMS Collaboration, “The CMS experiment at the CERN LHC”, *JINST* **3** (2008) S08004, doi:10.1088/1748-0221/3/08/S08004.
- [9] CMS Collaboration, “CMS luminosity based on pixel cluster counting – Summer 2013 update”, CMS Physics Analysis Summary CMS-PAS-LUM-13-001, 2013.
- [10] J. Alwall et al., “The automated computation of tree-level and next-to-leading order differential cross sections, and their matching to parton shower simulations”, *JHEP* **07** (2014) 079, doi:10.1007/JHEP07(2014)079, arXiv:1405.0301.
- [11] T. Sjöstrand, S. Mrenna, and P. Z. Skands, “PYTHIA 6.4 physics and manual”, *JHEP* **05** (2006) 026, doi:10.1088/1126-6708/2006/05/026, arXiv:hep-ph/0603175.
- [12] J. Pumplin, D. R. Stump, J. Huston, H. L. Lai, P. Nadolsky, and W. K. Tung, “New generation of parton distributions with uncertainties from global QCD analysis”, *JHEP* **07** (2002) 012, doi:10.1088/1126-6708/2002/07/012, arXiv:hep-ph/0201195.
- [13] GEANT4 Collaboration, “GEANT4 – a simulation toolkit”, *Nucl. Instrum. Meth. A* **506** (2003) 250, doi:10.1016/S0168-9002(03)01368-8.
- [14] CMS Collaboration, “Performance of electron reconstruction and selection with the CMS detector in proton-proton collisions at $\sqrt{s} = 8$ TeV”, *JINST* **10** (2015) P06005, doi:10.1088/1748-0221/10/06/P06005, arXiv:1502.02701.
- [15] CMS Collaboration, “Electron performance with 19.6 fb^{-1} of data at $\sqrt{s} = 8$ TeV with the CMS detector”, CMS Detector Performance Summary CMS-DP-2013-003, 2013.
- [16] CMS Collaboration, “Performance of CMS muon reconstruction in pp collision events at $\sqrt{s} = 7$ TeV”, *JINST* **7** (2012) P10002, doi:10.1088/1748-0221/7/10/P10002, arXiv:1206.4071.
- [17] CMS Collaboration, “Commissioning of the particle-flow event reconstruction with leptons from J/ψ and W decays at 7 TeV”, CMS Physics Analysis Summary CMS-PAS-PFT-10-003, 2010.

- [18] CMS Collaboration, “Commissioning of the particle–flow reconstruction in minimum–bias and jet events from pp collisions at 7 TeV”, CMS Physics Analysis Summary CMS-PAS-PFT-10-002, 2010.
- [19] M. Cacciari and G. P. Salam, “Dispelling the N^3 myth for the k_t jet-finder”, *Phys. Lett. B* **641** (2006) 57, doi:10.1016/j.physletb.2006.08.037, arXiv:hep-ph/0512210.
- [20] M. Cacciari, G. P. Salam, and G. Soyez, “The anti- k_t jet clustering algorithm”, *JHEP* **04** (2008) 063, doi:10.1088/1126-6708/2008/04/063, arXiv:0802.1189.
- [21] CMS Collaboration, “Pileup jet identification”, CMS Physics Analysis Summary CMS-PAS-JME-13-005, 2013.
- [22] M. Cacciari, G. P. Salam, and G. Soyez, “The catchment area of jets”, *JHEP* **04** (2008) 005, doi:10.1088/1126-6708/2008/04/005, arXiv:0802.1188.
- [23] M. Cacciari and G. P. Salam, “Pileup subtraction using jet areas”, *Phys. Lett. B* **659** (2008) 119, doi:10.1016/j.physletb.2007.09.077, arXiv:0707.1378.
- [24] CMS Collaboration, “Identification of b-quark jets with the CMS experiment”, *JINST* **8** (2012) P04013, doi:10.1088/1748-0221/8/04/P04013, arXiv:1211.4462.
- [25] CMS Collaboration, “Performance of b tagging at $\sqrt{s} = 8$ TeV in multijet, $t\bar{t}$ and boosted topology events”, CMS Physics Analysis Summary CMS-PAS-BTV-13-001, 2013.
- [26] CMS Collaboration, “Determination of jet energy calibration and transverse momentum resolution in CMS”, *JINST* **6** (2011) P11002, doi:10.1088/1748-0221/6/11/P11002, arXiv:1107.4277.
- [27] CMS Collaboration, “Search for the associated production of the Higgs boson with a top-quark pair”, *JHEP* **09** (2014) 087, doi:10.1007/JHEP09(2014)087, arXiv:1408.1682. [Erratum: doi:10.1007/JHEP10(2014)106].
- [28] M. Czakon, P. Fiedler, and A. Mitov, “Total top-quark pair-production cross section at hadron colliders through $\mathcal{O}(\alpha_S^4)$ ”, *Phys. Rev. Lett.* **110** (2013) 252004, doi:10.1103/PhysRevLett.110.252004, arXiv:1303.6254.
- [29] R. Gavin, Y. Li, F. Petriello, and S. Quackenbush, “FEWZ 2.0: A code for hadronic Z production at next-to-next-to-leading order”, *Comp. Phys. Comm.* **182** (2011) 2388, doi:10.1016/j.cpc.2011.06.008, arXiv:1011.3540.
- [30] LHC Higgs Cross Section Working Group, “Handbook of LHC Higgs cross sections: 3. Higgs properties”, CERN Report CERN-2013-004, 2013. doi:10.5170/CERN-2013-004, arXiv:1307.1347.
- [31] K. Melnikov, M. Schulze, and A. Scharf, “QCD corrections to top quark pair production in association with a photon at hadron colliders”, *Phys. Rev. D* **83** (2011) 074013, doi:10.1103/PhysRevD.83.074013, arXiv:1102.1967.
- [32] J. M. Campbell and R. K. Ellis, “MCFM for the Tevatron and the LHC”, *Nucl. Phys. B - Proceedings Supplements* **205** (2010) 10, doi:10.1016/j.nuclphysbps.2010.08.011, arXiv:1007.3492. Proceedings of the 10th DESY Workshop on Elementary Particle Theory.

- [33] N. Kidonakis, “NNLL threshold resummation for top-pair and single-top production”, *Phys. Part. Nucl.* **45** (2014) 714, doi:10.1134/S1063779614040091, arXiv:1210.7813.
- [34] CMS Collaboration, “Measurement of differential top-quark pair production cross sections in pp collisions at $\sqrt{s} = 7$ TeV”, *Eur. Phys. J. C* **73** (2013) 2339, doi:10.1140/epjc/s10052-013-2339-4, arXiv:1211.2220.
- [35] B. P. Roe et al., “Boosted decision trees as an alternative to artificial neural networks for particle identification”, *Nucl. Instrum. Meth. A* **543** (2005) 577, doi:10.1016/j.nima.2004.12.018, arXiv:physics/0408124.
- [36] CMS Collaboration, “Measurement of the inelastic proton-proton cross section at $\sqrt{s} = 7$ TeV”, *Phys. Lett. B* **722** (2013) 5, doi:10.1016/j.physletb.2013.03.024, arXiv:1210.6718.
- [37] S. Alekhin et al., “The PDF4LHC Working Group interim report”, (2011). arXiv:1101.0536.
- [38] M. Botje et al., “The PDF4LHC Working Group interim recommendations”, (2011). arXiv:1101.0538.
- [39] A. Bredenstein, A. Denner, S. Dittmaier, and S. Pozzorini, “NLO QCD corrections to $t\bar{t}b\bar{b}$ production at the LHC: 2. Full hadronic results”, *JHEP* **03** (2010) 021, doi:10.1007/JHEP03(2010)021, arXiv:1001.4006.
- [40] LHC Higgs Combination Group, “Procedure for the LHC Higgs boson search combination in Summer 2011”, Technical Report CMS-NOTE-2011-005, ATL-PHYS-PUB-2011-11, 2011.
- [41] CMS Collaboration, “Observation of a new boson at a mass of 125 GeV with the CMS experiment at the LHC”, *Phys. Lett. B* **716** (2012) 30, doi:10.1016/j.physletb.2012.08.021, arXiv:1207.7235.
- [42] G. Cowan, K. Cranmer, E. Gross, and O. Vitells, “Asymptotic formulae for likelihood-based tests of new physics”, *Eur. Phys. J. C* **71** (2011) 1554, doi:10.1140/epjc/s10052-011-1554-0, arXiv:1007.1727.
- [43] J. M. Campbell and R. K. Ellis, “ $t\bar{t}W^\pm$ production and decay at NLO”, *JHEP* **07** (2012) 052, doi:10.1007/JHEP07(2012)052, arXiv:1204.5678.
- [44] W. Buchmuller and D. Wyler, “Effective Lagrangian Analysis of New Interactions and Flavor Conservation”, *Nucl. Phys. B* **268** (1986) 621, doi:10.1016/0550-3213(86)90262-2.
- [45] E. L. Berger, Q.-H. Cao, and I. Low, “Model independent constraints among the Wtb , $Zb\bar{b}$, and $Zt\bar{t}$ Couplings”, *Phys. Rev. D* **80** (2009) 074020, doi:10.1103/PhysRevD.80.074020, arXiv:0907.2191.
- [46] B. Grzadkowski, M. Iskrzynski, M. Misiak, and J. Rosiek, “Dimension-six terms in the Standard Model lagrangian”, *JHEP* **10** (2010) 085, doi:10.1007/JHEP10(2010)085, arXiv:1008.4884.

- [47] A. Alloul, B. Fuks, and V. Sanz, “Phenomenology of the Higgs effective lagrangian via FEYNRULES”, *JHEP* **04** (2014) 110, doi:10.1007/JHEP04(2014)110, arXiv:1310.5150.
- [48] DELPHI Collaboration, “A Study of $b\bar{b}$ production in e^+e^- collisions at $\sqrt{s} = 130\text{--}207\text{ GeV}$ ”, *Eur. Phys. J. C* **60** (2009) 1, doi:10.1140/epjc/s10052-009-0917-2, arXiv:0901.4461.
- [49] ALEPH Collaboration, “A measurement of R_b using a lifetime mass tag”, *Phys. Lett. B* **401** (1997) 150, doi:10.1016/S0370-2693(97)00406-1.
- [50] DELPHI Collaboration, “A precise measurement of the partial decay width ratio $R_b^0 = \Gamma_{b\bar{b}}/\Gamma_{\text{had}}$ ”, *Eur. Phys. J. C* **10** (1999) 415, doi:10.1007/s100520050766.
- [51] L3 Collaboration, “Measurement of R_b and $\text{Br}(b \rightarrow \ell^0 X)$ at LEP using double-tag methods”, *Eur. Phys. J. C* **13** (2000) 47, doi:10.1007/s100520000296, arXiv:hep-ex/9909045.
- [52] OPAL Collaboration, “A measurement of R_b using a double tagging method”, *Eur. Phys. J. C* **8** (1999) 217, doi:10.1007/s100529901087, arXiv:hep-ex/9810002.
- [53] SLD Collaboration, “Measurement of the branching ratio of the Z^0 into heavy quarks”, *Phys. Rev. D* **71** (2005) 112004, doi:10.1103/PhysRevD.71.112004, arXiv:hep-ex/0503005.
- [54] R. Rontsch and M. Schulze, “Constraining couplings of top quarks to the Z boson in $t\bar{t} + Z$ production at the LHC”, *JHEP* **07** (2014) 091, doi:10.1007/JHEP07(2014)091, arXiv:1404.1005.
- [55] J. Ellis, V. Sanz, and T. You, “Complete Higgs sector constraints on dimension-6 operators”, *JHEP* **07** (2014) 036, doi:10.1007/JHEP07(2014)036, arXiv:1404.3667.
- [56] K. Whisnant, J.-M. Yang, B.-L. Young, and X. Zhang, “Dimension-six CP conserving operators of the third family quarks and their effects on collider observables”, *Phys. Rev. D* **56** (1997) 467, doi:10.1103/PhysRevD.56.467, arXiv:hep-ph/9702305.
- [57] E. Malkawi and C.-P. Yuan, “A global analysis of the top quark couplings to gauge bosons”, *Phys. Rev. D* **50** (1994) 4462, doi:10.1103/PhysRevD.50.4462, arXiv:hep-ph/9405322.
- [58] C. Zhang, N. Greiner, and S. Willenbrock, “Constraints on non-standard top quark couplings”, *Phys. Rev. D* **86** (2012) 014024, doi:10.1103/PhysRevD.86.014024, arXiv:1201.6670.
- [59] A. Tonerer and R. Rosenfeld, “Dipole-induced anomalous top quark couplings at the LHC”, *Phys. Rev. D* **90** (2014) 017701, doi:10.1103/PhysRevD.90.017701, arXiv:1404.2581.
- [60] A. Alloul et al., “FeynRules 2.0 – a complete toolbox for tree-level phenomenology”, *Comput. Phys. Commun.* **185** (2014) 2250, doi:10.1016/j.cpc.2014.04.012, arXiv:1310.1921.

A Input variables to linear discriminant for event reconstruction

Table 10: Variables used to match leptons and jets to their parent particles in reconstructing $t\bar{t}W$, $t\bar{t}Z$, and $t\bar{t}$ events. In $t\bar{t}Z$ events, the two leptons matched to the Z boson decay are removed and the remaining $t\bar{t}$ system is reconstructed. In $t\bar{t}W$ events, the $t\bar{t}$ system is reconstructed with the leptons that best match the $t\bar{t}$ decay, and the lepton from the associated W boson (and any variables with p_T^{miss}) are not used. In $t\bar{t}$ events, ℓ_b denotes a lepton from b -hadron decay.

Reconstructed event	Decay products of the $t\bar{t}$ system				
	$bq\bar{q} \bar{b}q\bar{q}$	$b\ell\nu \bar{b}q\bar{q}$	$b\ell\nu \bar{b}\ell\nu$	$\ell_b q\bar{q} \bar{b}\ell\nu$	$\ell_b \ell\nu \bar{b}\ell\nu$
OS dilepton $t\bar{t}Z$	X				
SS dilepton $t\bar{t}W$		X			
3ℓ $t\bar{t}Z$		X			
3ℓ $t\bar{t}W$			X		
OS dilepton $t\bar{t}$			X		
SS dilepton $t\bar{t}$				X	
3ℓ $t\bar{t}$					X
Input variables					
<i>Jet CSV (b tag) discriminator</i>					
b jet CSV	X	X	X	X	X
Higher jet CSV from $W \rightarrow q\bar{q}$	X	X		X	
Lower jet CSV from $W \rightarrow q\bar{q}$	X	X		X	
<i>Jet charge</i>					
Charge of b jet from t	X		X		
Charge of b jet from \bar{t}	X		X		
Charge of b jet from t $\rightarrow b\ell\nu$		X			
Charge of b jet from t $\rightarrow bq\bar{q}$		X			
Charge of b jet not decaying to a lepton				X	X
Sum of charges of jets from $W \rightarrow q\bar{q}$	X	X		X	
<i>Invariant mass</i>					
Mass of lepton and b jet from t			X		
Mass of lepton and b jet from \bar{t}			X		
Mass of lepton and b jet from t $\rightarrow b\ell\nu$		X		X	X
Mass of leptons from t $\rightarrow \ell_b \ell\nu$					X
M_T of \vec{p}_T^{miss} and \vec{p}_T of lepton and b jet from t		X		X	
Mass of two jets from $W \rightarrow q\bar{q}$	X	X		X	
Mass of b jet and quark jets from t $\rightarrow bq\bar{q}$	X	X			
Mass of lepton from b and jets from t $\rightarrow \ell_b q\bar{q}$				X	
Ratio of M_T to mass for jets from t or W	X	X	X		

B Input variables to final discriminants (BDTs)

Table 11: Input variables to the BDT that distinguishes SS $t\bar{t}W$ from $t\bar{t}$, ranked by signal-background separation.

BDT inputs: SS $t\bar{t}W$ vs. $t\bar{t}$	3 jet	≥ 4 jets
M_T of \vec{p}_T^{miss} and \vec{p}_T of leptons and jets	1	1
p_T^{miss}	4	2
Second-highest lepton p_T	6	3
Match score for $t\bar{t} \rightarrow \ell_b q \bar{q} \bar{\ell} \nu$	2	4
Highest lepton p_T	5	5
Second-highest CSV value of a jet	8	6
$t\bar{t}$ matched top quark M_T from $b\nu$	7	7
Match score for $t\bar{t}W \rightarrow b\nu \bar{b}q$	9	8
Match score for $t\bar{t}W \rightarrow b\nu \bar{b}q\bar{q}$	—	9
$t\bar{t}$ matched top quark mass from $\ell_b q \bar{q}$	3	—

Table 12: Input variables to BDT that distinguishes 3ℓ $t\bar{t}W$ from $t\bar{t}$, ranked by signal-background separation.

BDT inputs: 3ℓ $t\bar{t}W$ vs. $t\bar{t}$	1 jet	≥ 2 jets
Second-highest CSV value of a jet	—	1
M_T of \vec{p}_T^{miss} and \vec{p}_T of leptons and jets	1	2
Match score for $t\bar{t}W \rightarrow \ell\nu b\ell\nu \bar{\ell}\nu$	—	3
Second-highest SS lepton p_T	4	4
$t\bar{t}$ matched top quark mass from ℓ_W and ℓ_b	—	5
Highest SS lepton p_T	3	6
Match score for $t\bar{t}W \rightarrow \ell\nu b\ell\nu \ell\nu$	2	—
p_T^{miss}	5	—
Jet p_T	6	—

Table 13: Input variables to BDT that distinguishes 3ℓ $t\bar{t}Z$ from WZ and $t\bar{t}$, ranked by signal-background separation.

BDT inputs: 3ℓ $t\bar{t}Z$ vs. WZ and $t\bar{t}$	3 jet	≥ 4 jets
Match score for $t\bar{t}Z \rightarrow \ell\ell b\ell\bar{b}q$	1	1
Match score for $t\bar{t}Z \rightarrow \ell\ell b\ell\bar{b}q\bar{q}$	—	2
Match score for $t\bar{t}Z \rightarrow \ell\ell \ell\bar{\nu}\bar{b}q\bar{q}$	8	3
Match score for $t\bar{t}Z \rightarrow \ell\ell b\ell\bar{b}q\bar{q}$	9	4
Number of medium b-tagged jets	3	5
Mass of lepton pair matched to Z boson	7	6
M_T of \vec{p}_T^{miss} and \vec{p}_T of leptons and jets	4	7
Match score for $t\bar{t}Z \rightarrow \ell\ell b\ell\bar{b}$	2	—
Match score for $t\bar{t}Z \rightarrow \ell\ell \ell\bar{\nu}\bar{b}q$	5	—
Match score for $t\bar{t}Z \rightarrow \ell\ell b\ell\bar{b}q$	6	—

Table 14: Input variables to BDT that distinguishes OS $t\bar{t}Z$ from $t\bar{t}$ (used as input to the final discriminant), ranked by signal-background separation.

BDT inputs: OS $t\bar{t}Z$ vs. $t\bar{t}$	5 jet	≥ 6 jets
ΔR between leptons	1	1
p_T of dilepton system	2	2
Dilepton invariant mass	3	3
H_T^{miss}	4	4
Match score for $t\bar{t} \rightarrow b\ell\bar{\nu}\bar{b}\ell\bar{\nu}$	5	5
Number of jets with $p_T > 40$ GeV	9	6
Match score for $t\bar{t}Z \rightarrow \ell\ell bq\bar{q}\bar{b}q\bar{q}$	—	7
Match score for $t\bar{t}Z \rightarrow \ell\ell bq\bar{q}\bar{b}q\bar{q}$	8	8
Match score for $t\bar{t}Z \rightarrow \ell\ell bq\bar{q}\bar{b}q$	7	9
Ratio of M_T to mass of jets	6	10
CSV of jet matched to b from $t\bar{t}$	11	11
CSV of jet matched to \bar{b} from $t\bar{t}$	10	12

Table 15: Input variables to BDT that distinguishes OS $t\bar{t}Z$ from Z boson and $t\bar{t}$ (the final discriminant), ranked by signal-background separation.

BDT inputs: OS $t\bar{t}Z$ vs. Z and $t\bar{t}$	5 jet	≥ 6 jets
OS $t\bar{t}Z$ vs. $t\bar{t}$ BDT	1	1
Match score for $t\bar{t}Z \rightarrow \ell\ell bq\bar{q}\bar{b}q\bar{q}$	3	2
Match score for $t\bar{t}Z \rightarrow \ell\ell bq\bar{q}\bar{b}q$	4	3
Match score for $t\bar{t}Z \rightarrow \ell\ell bq\bar{q}\bar{b}q\bar{q}$	—	4
Minimum χ^2 for $t\bar{t}Z \rightarrow \ell\ell bq\bar{q}\bar{b}q\bar{q}$	—	5
Number of jets with $p_T > 40$ GeV	6	6
Fifth-highest jet p_T	5	7
Ratio of M_T to mass of jets and leptons	2	8
Second-highest jet CSV	7	9
Highest jet CSV	8	10

C The CMS Collaboration

Yerevan Physics Institute, Yerevan, Armenia

V. Khachatryan, A.M. Sirunyan, A. Tumasyan

Institut für Hochenergiephysik der OeAW, Wien, Austria

W. Adam, E. Asilar, T. Bergauer, J. Brandstetter, E. Brondolin, M. Dragicevic, J. Erö, M. Flechl, M. Friedl, R. Frühwirth¹, V.M. Ghete, C. Hartl, N. Hörmann, J. Hrubec, M. Jeitler¹, V. Knünz, A. König, M. Krammer¹, I. Krätschmer, D. Liko, T. Matsushita, I. Mikulec, D. Rabady², B. Rahbaran, H. Rohringer, J. Schieck¹, R. Schöfbeck, J. Strauss, W. Treberer-Treberspurg, W. Waltenberger, C.-E. Wulz¹

National Centre for Particle and High Energy Physics, Minsk, Belarus

V. Mossolov, N. Shumeiko, J. Suarez Gonzalez

Universiteit Antwerpen, Antwerpen, Belgium

S. Alderweireldt, T. Cornelis, E.A. De Wolf, X. Janssen, A. Knutsson, J. Lauwers, S. Luyckx, R. Rougny, M. Van De Klundert, H. Van Haevermaet, P. Van Mechelen, N. Van Remortel, A. Van Spilbeeck

Vrije Universiteit Brussel, Brussel, Belgium

S. Abu Zeid, F. Blekman, J. D'Hondt, N. Daci, I. De Bruyn, K. Deroover, N. Heracleous, J. Keaveney, S. Lowette, L. Moreels, A. Olbrechts, Q. Python, D. Strom, S. Tavernier, W. Van Doninck, P. Van Mulders, G.P. Van Onsem, I. Van Parijs

Université Libre de Bruxelles, Bruxelles, Belgium

P. Barria, H. Brun, C. Caillol, B. Clerboux, G. De Lentdecker, G. Fasanella, L. Favart, A. Grebenyuk, G. Karapostoli, T. Lenzi, A. Léonard, T. Maerschalk, A. Marinov, L. Perniè, A. Randle-conde, T. Reis, T. Seva, C. Vander Velde, P. Vanlaer, R. Yonamine, F. Zenoni, F. Zhang³

Ghent University, Ghent, Belgium

K. Beernaert, L. Benucci, A. Cimmino, S. Crucy, D. Dobur, A. Fagot, G. Garcia, M. Gul, J. Mccartin, A.A. Ocampo Rios, D. Poyraz, D. Ryckbosch, S. Salva, M. Sigamani, N. Strobbe, M. Tytgat, W. Van Driessche, E. Yazgan, N. Zaganidis

Université Catholique de Louvain, Louvain-la-Neuve, Belgium

S. Basegmez, C. Beluffi⁴, O. Bondu, S. Brochet, G. Bruno, A. Caudron, L. Ceard, G.G. Da Silveira, C. Delaere, D. Favart, L. Forthomme, A. Giammanco⁵, J. Hollar, A. Jafari, P. Jez, M. Komm, V. Lemaître, A. Mertens, C. Nuttens, L. Perrini, A. Pin, K. Piotrkowski, A. Popov⁶, L. Quertenmont, M. Selvaggi, M. Vidal Marono

Université de Mons, Mons, Belgium

N. Beliy, G.H. Hammad

Centro Brasileiro de Pesquisas Fisicas, Rio de Janeiro, Brazil

W.L. Aldá Júnior, G.A. Alves, L. Brito, M. Correa Martins Junior, M. Hamer, C. Hensel, C. Mora Herrera, A. Moraes, M.E. Pol, P. Rebello Teles

Universidade do Estado do Rio de Janeiro, Rio de Janeiro, Brazil

E. Belchior Batista Das Chagas, W. Carvalho, J. Chinellato⁷, A. Custódio, E.M. Da Costa, D. De Jesus Damiao, C. De Oliveira Martins, S. Fonseca De Souza, L.M. Huertas Guativa, H. Malbouisson, D. Matos Figueiredo, L. Mundim, H. Nogima, W.L. Prado Da Silva, A. Santoro, A. Sznajder, E.J. Tonelli Manganote⁷, A. Vilela Pereira

Universidade Estadual Paulista ^a, Universidade Federal do ABC ^b, São Paulo, Brazil

S. Ahuja^a, C.A. Bernardes^b, A. De Souza Santos^b, S. Dogra^a, T.R. Fernandez Perez Tomei^a, E.M. Gregores^b, P.G. Mercadante^b, C.S. Moon^{a,8}, S.F. Novaes^a, Sandra S. Padula^a, D. Romero Abad, J.C. Ruiz Vargas

Institute for Nuclear Research and Nuclear Energy, Sofia, Bulgaria

A. Aleksandrov, R. Hadjiiska, P. Iaydjiev, M. Rodozov, S. Stoykova, G. Sultanov, M. Vutova

University of Sofia, Sofia, Bulgaria

A. Dimitrov, I. Glushkov, L. Litov, B. Pavlov, P. Petkov

Institute of High Energy Physics, Beijing, China

M. Ahmad, J.G. Bian, G.M. Chen, H.S. Chen, M. Chen, T. Cheng, R. Du, C.H. Jiang, R. Plestina⁹, F. Romeo, S.M. Shaheen, J. Tao, C. Wang, Z. Wang, H. Zhang

State Key Laboratory of Nuclear Physics and Technology, Peking University, Beijing, China

C. Asawatangtrakuldee, Y. Ban, Q. Li, S. Liu, Y. Mao, S.J. Qian, D. Wang, Z. Xu

Universidad de Los Andes, Bogota, Colombia

C. Avila, A. Cabrera, L.F. Chaparro Sierra, C. Florez, J.P. Gomez, B. Gomez Moreno, J.C. Sanabria

University of Split, Faculty of Electrical Engineering, Mechanical Engineering and Naval Architecture, Split, Croatia

N. Godinovic, D. Lelas, I. Puljak, P.M. Ribeiro Cipriano

University of Split, Faculty of Science, Split, Croatia

Z. Antunovic, M. Kovac

Institute Rudjer Boskovic, Zagreb, Croatia

V. Brigljevic, K. Kadija, J. Luetic, S. Micanovic, L. Sudic

University of Cyprus, Nicosia, Cyprus

A. Attikis, G. Mavromanolakis, J. Mousa, C. Nicolaou, F. Ptochos, P.A. Razis, H. Rykaczewski

Charles University, Prague, Czech Republic

M. Bodlak, M. Finger¹⁰, M. Finger Jr.¹⁰

Academy of Scientific Research and Technology of the Arab Republic of Egypt, Egyptian Network of High Energy Physics, Cairo, Egypt

A.A. Abdelalim^{11,12}, A. Awad^{13,14}, M.A. Mahmoud^{15,15}, A. Mahrous¹¹, A. Radi^{14,13}

National Institute of Chemical Physics and Biophysics, Tallinn, Estonia

B. Calpas, M. Kadastik, M. Murumaa, M. Raidal, A. Tiko, C. Veelken

Department of Physics, University of Helsinki, Helsinki, Finland

P. Eerola, J. Pekkanen, M. Voutilainen

Helsinki Institute of Physics, Helsinki, Finland

J. Härkönen, V. Karimäki, R. Kinnunen, T. Lampén, K. Lassila-Perini, S. Lehti, T. Lindén, P. Luukka, T. Mäenpää, T. Peltola, E. Tuominen, J. Tuominiemi, E. Tuovinen, L. Wendland

Lappeenranta University of Technology, Lappeenranta, Finland

J. Talvitie, T. Tuuva

DSM/IRFU, CEA/Saclay, Gif-sur-Yvette, France

M. Besancon, F. Couderc, M. Dejardin, D. Denegri, B. Fabbro, J.L. Faure, C. Favaro, F. Ferri,

S. Ganjour, A. Givernaud, P. Gras, G. Hamel de Monchenault, P. Jarry, E. Locci, M. Machet, J. Malcles, J. Rander, A. Rosowsky, M. Titov, A. Zghiche

Laboratoire Leprince-Ringuet, Ecole Polytechnique, IN2P3-CNRS, Palaiseau, France

I. Antropov, S. Baffioni, F. Beaudette, P. Busson, L. Cadamuro, E. Chapon, C. Charlot, T. Dahms, O. Davignon, N. Filipovic, A. Florent, R. Granier de Cassagnac, S. Lisniak, L. Mastrolorenzo, P. Miné, I.N. Naranjo, M. Nguyen, C. Ochando, G. Ortona, P. Paganini, P. Pigard, S. Regnard, R. Salerno, J.B. Sauvan, Y. Sirois, T. Strebler, Y. Yilmaz, A. Zabi

Institut Pluridisciplinaire Hubert Curien, Université de Strasbourg, Université de Haute Alsace Mulhouse, CNRS/IN2P3, Strasbourg, France

J.-L. Agram¹⁶, J. Andrea, A. Aubin, D. Bloch, J.-M. Brom, M. Buttignol, E.C. Chabert, N. Chanon, C. Collard, E. Conte¹⁶, X. Coubez, J.-C. Fontaine¹⁶, D. Gelé, U. Goerlach, C. Goetzmann, A.-C. Le Bihan, J.A. Merlin², K. Skovpen, P. Van Hove

Centre de Calcul de l'Institut National de Physique Nucleaire et de Physique des Particules, CNRS/IN2P3, Villeurbanne, France

S. Gadrat

Université de Lyon, Université Claude Bernard Lyon 1, CNRS-IN2P3, Institut de Physique Nucléaire de Lyon, Villeurbanne, France

S. Beauceron, C. Bernet, G. Boudoul, E. Bouvier, C.A. Carrillo Montoya, R. Chierici, D. Contardo, B. Courbon, P. Depasse, H. El Mamouni, J. Fan, J. Fay, S. Gascon, M. Gouzevitch, B. Ille, F. Lagarde, I.B. Laktineh, M. Lethuillier, L. Mirabito, A.L. Pequegnot, S. Perries, J.D. Ruiz Alvarez, D. Sabes, L. Sgandurra, V. Sordini, M. Vander Donckt, P. Verdier, S. Viret

Georgian Technical University, Tbilisi, Georgia

T. Toriashvili¹⁷

Tbilisi State University, Tbilisi, Georgia

Z. Tsamalaidze¹⁰

RWTH Aachen University, I. Physikalisches Institut, Aachen, Germany

C. Autermann, S. Beranek, M. Edelhoff, L. Feld, A. Heister, M.K. Kiesel, K. Klein, M. Lipinski, A. Ostapchuk, M. Preuten, F. Raupach, S. Schael, J.F. Schulte, T. Verlage, H. Weber, B. Wittmer, V. Zhukov⁶

RWTH Aachen University, III. Physikalisches Institut A, Aachen, Germany

M. Ata, M. Brodski, E. Dietz-Laursonn, D. Duchardt, M. Endres, M. Erdmann, S. Erdweg, T. Esch, R. Fischer, A. Güth, T. Hebbeker, C. Heidemann, K. Hoepfner, D. Klingebiel, S. Knutzen, P. Kreuzer, M. Merschmeyer, A. Meyer, P. Millet, M. Olschewski, K. Padeken, P. Papacz, T. Pook, M. Radziej, H. Reithler, M. Rieger, F. Scheuch, L. Sonnenschein, D. Teysier, S. Thüer

RWTH Aachen University, III. Physikalisches Institut B, Aachen, Germany

V. Cherepanov, Y. Erdogan, G. Flügge, H. Geenen, M. Geisler, F. Hoehle, B. Kargoll, T. Kress, Y. Kuessel, A. Künsken, J. Lingemann², A. Nehr Korn, A. Nowack, I.M. Nugent, C. Pistone, O. Pooth, A. Stahl

Deutsches Elektronen-Synchrotron, Hamburg, Germany

M. Aldaya Martin, I. Asin, N. Bartosik, O. Behnke, U. Behrens, A.J. Bell, K. Borras¹⁸, A. Burgmeier, A. Cakir, L. Calligaris, A. Campbell, S. Choudhury, F. Costanza, C. Diez Pardos, G. Dolinska, S. Dooling, T. Dorland, G. Eckerlin, D. Eckstein, T. Eichhorn, G. Flucke, E. Gallo¹⁹, J. Garay Garcia, A. Geiser, A. Gizhko, P. Gunnellini, J. Hauk, M. Hempel²⁰, H. Jung,

A. Kalogeropoulos, O. Karacheban²⁰, M. Kasemann, P. Katsas, J. Kieseler, C. Kleinwort, I. Korol, W. Lange, J. Leonard, K. Lipka, A. Lobanov, W. Lohmann²⁰, R. Mankel, I. Marfin²⁰, I.-A. Melzer-Pellmann, A.B. Meyer, G. Mittag, J. Mnich, A. Mussgiller, S. Naumann-Emme, A. Nayak, E. Ntomari, H. Perrey, D. Pitzl, R. Placakyte, A. Raspereza, B. Roland, M.Ö. Sahin, P. Saxena, T. Schoerner-Sadenius, M. Schröder, C. Seitz, S. Spannagel, K.D. Trippkewitz, R. Walsh, C. Wissing

University of Hamburg, Hamburg, Germany

V. Blobel, M. Centis Vignali, A.R. Draeger, J. Erfle, E. Garutti, K. Goebel, D. Gonzalez, M. Görner, J. Haller, M. Hoffmann, R.S. Höing, A. Junkes, R. Klanner, R. Kogler, T. Lapsien, T. Lenz, I. Marchesini, D. Marconi, M. Meyer, D. Nowatschin, J. Ott, F. Pantaleo², T. Peiffer, A. Perieanu, N. Pietsch, J. Poehlsen, D. Rathjens, C. Sander, H. Schettler, P. Schleper, E. Schlieckau, A. Schmidt, J. Schwandt, M. Seidel, V. Sola, H. Stadie, G. Steinbrück, H. Tholen, D. Troendle, E. Usai, L. Vanelderden, A. Vanhoefer, B. Vormwald

Institut für Experimentelle Kernphysik, Karlsruhe, Germany

M. Akbiyik, C. Barth, C. Baus, J. Berger, C. Böser, E. Butz, T. Chwalek, F. Colombo, W. De Boer, A. Descroix, A. Dierlamm, S. Fink, F. Frensch, M. Giffels, A. Gilbert, F. Hartmann², S.M. Heindl, U. Husemann, I. Katkov⁶, A. Kornmayer², P. Lobelle Pardo, B. Maier, H. Mildner, M.U. Mozer, T. Müller, Th. Müller, M. Plagge, G. Quast, K. Rabbertz, S. Röcker, F. Roscher, H.J. Simonis, F.M. Stober, R. Ulrich, J. Wagner-Kuhr, S. Wayand, M. Weber, T. Weiler, C. Wöhrmann, R. Wolf

Institute of Nuclear and Particle Physics (INPP), NCSR Demokritos, Aghia Paraskevi, Greece

G. Anagnostou, G. Daskalakis, T. Gerasis, V.A. Giakoumopoulou, A. Kyriakis, D. Loukas, A. Psallidas, I. Topsis-Giotis

University of Athens, Athens, Greece

A. Agapitos, S. Kesisoglou, A. Panagiotou, N. Saoulidou, E. Tziaferi

University of Ioánnina, Ioánnina, Greece

I. Evangelou, G. Flouris, C. Foudas, P. Kokkas, N. Loukas, N. Manthos, I. Papadopoulos, E. Paradas, J. Strologas

Wigner Research Centre for Physics, Budapest, Hungary

G. Bencze, C. Hajdu, A. Hazi, P. Hidas, D. Horvath²¹, F. Sikler, V. Veszpremi, G. Vesztergombi²², A.J. Zsigmond

Institute of Nuclear Research ATOMKI, Debrecen, Hungary

N. Beni, S. Czellar, J. Karancsi²³, J. Molnar, Z. Szillasi

University of Debrecen, Debrecen, Hungary

M. Bartók²⁴, A. Makovec, P. Raics, Z.L. Trocsanyi, B. Ujvari

National Institute of Science Education and Research, Bhubaneswar, India

P. Mal, K. Mandal, D.K. Sahoo, N. Sahoo, S.K. Swain

Panjab University, Chandigarh, India

S. Bansal, S.B. Beri, V. Bhatnagar, R. Chawla, R. Gupta, U. Bhawandeep, A.K. Kalsi, A. Kaur, M. Kaur, R. Kumar, A. Mehta, M. Mittal, J.B. Singh, G. Walia

University of Delhi, Delhi, India

Ashok Kumar, A. Bhardwaj, B.C. Choudhary, R.B. Garg, A. Kumar, S. Malhotra, M. Naimuddin, N. Nishu, K. Ranjan, R. Sharma, V. Sharma

Saha Institute of Nuclear Physics, Kolkata, India

S. Bhattacharya, K. Chatterjee, S. Dey, S. Dutta, Sa. Jain, N. Majumdar, A. Modak, K. Mondal, S. Mukherjee, S. Mukhopadhyay, A. Roy, D. Roy, S. Roy Chowdhury, S. Sarkar, M. Sharan

Bhabha Atomic Research Centre, Mumbai, India

A. Abdulsalam, R. Chudasama, D. Dutta, V. Jha, V. Kumar, A.K. Mohanty², L.M. Pant, P. Shukla, A. Topkar

Tata Institute of Fundamental Research, Mumbai, India

T. Aziz, S. Banerjee, S. Bhowmik²⁵, R.M. Chatterjee, R.K. Dewanjee, S. Dugad, S. Ganguly, S. Ghosh, M. Guchait, A. Gurtu²⁶, G. Kole, S. Kumar, B. Mahakud, M. Maity²⁵, G. Majumder, K. Mazumdar, S. Mitra, G.B. Mohanty, B. Parida, T. Sarkar²⁵, K. Sudhakar, N. Sur, B. Sutar, N. Wickramage²⁷

Indian Institute of Science Education and Research (IISER), Pune, India

S. Chauhan, S. Dube, S. Sharma

Institute for Research in Fundamental Sciences (IPM), Tehran, Iran

H. Bakhshiansohi, H. Behnamian, S.M. Etesami²⁸, A. Fahim²⁹, R. Goldouzian, M. Khakzad, M. Mohammadi Najafabadi, M. Naseri, S. Paktinat Mehdiabadi, F. Rezaei Hosseinabadi, B. Safarzadeh³⁰, M. Zeinali

University College Dublin, Dublin, Ireland

M. Felcini, M. Grunewald

INFN Sezione di Bari ^a, Università di Bari ^b, Politecnico di Bari ^c, Bari, Italy

M. Abbrescia^{a,b}, C. Calabria^{a,b}, C. Caputo^{a,b}, A. Colaleo^a, D. Creanza^{a,c}, L. Cristella^{a,b}, N. De Filippis^{a,c}, M. De Palma^{a,b}, L. Fiore^a, G. Iaselli^{a,c}, G. Maggi^{a,c}, M. Maggi^a, G. Miniello^{a,b}, S. My^{a,c}, S. Nuzzo^{a,b}, A. Pompili^{a,b}, G. Pugliese^{a,c}, R. Radogna^{a,b}, A. Ranieri^a, G. Selvaggi^{a,b}, L. Silvestris^{a,2}, R. Venditti^{a,b}, P. Verwilligen^a

INFN Sezione di Bologna ^a, Università di Bologna ^b, Bologna, Italy

G. Abbiendi^a, C. Battilana², A.C. Benvenuti^a, D. Bonacorsi^{a,b}, S. Braibant-Giacomelli^{a,b}, L. Brigliadori^{a,b}, R. Campanini^{a,b}, P. Capiluppi^{a,b}, A. Castro^{a,b}, F.R. Cavallo^a, S.S. Chhibra^{a,b}, G. Codispoti^{a,b}, M. Cuffiani^{a,b}, G.M. Dallavalle^a, F. Fabbri^a, A. Fanfani^{a,b}, D. Fasanella^{a,b}, P. Giacomelli^a, C. Grandi^a, L. Guiducci^{a,b}, S. Marcellini^a, G. Masetti^a, A. Montanari^a, F.L. Navarria^{a,b}, A. Perrotta^a, A.M. Rossi^{a,b}, T. Rovelli^{a,b}, G.P. Siroli^{a,b}, N. Tosi^{a,b}, R. Travaglini^{a,b}

INFN Sezione di Catania ^a, Università di Catania ^b, Catania, Italy

G. Cappello^a, M. Chiorboli^{a,b}, S. Costa^{a,b}, F. Giordano^{a,b}, R. Potenza^{a,b}, A. Tricomi^{a,b}, C. Tuve^{a,b}

INFN Sezione di Firenze ^a, Università di Firenze ^b, Firenze, Italy

G. Barbagli^a, V. Ciulli^{a,b}, C. Civinini^a, R. D'Alessandro^{a,b}, E. Focardi^{a,b}, S. Gonzi^{a,b}, V. Gori^{a,b}, P. Lenzi^{a,b}, M. Meschini^a, S. Paoletti^a, G. Sguazzoni^a, A. Tropiano^{a,b}, L. Viliani^{a,b}

INFN Laboratori Nazionali di Frascati, Frascati, Italy

L. Benussi, S. Bianco, F. Fabbri, D. Piccolo, F. Primavera

INFN Sezione di Genova ^a, Università di Genova ^b, Genova, Italy

V. Calvelli^{a,b}, F. Ferro^a, M. Lo Vetere^{a,b}, M.R. Monge^{a,b}, E. Robutti^a, S. Tosi^{a,b}

INFN Sezione di Milano-Bicocca ^a, Università di Milano-Bicocca ^b, Milano, Italy

L. Brianza, M.E. Dinardo^{a,b}, S. Fiorendi^{a,b}, S. Gennai^a, R. Gerosa^{a,b}, A. Ghezzi^{a,b}, P. Govoni^{a,b},

S. Malvezzi^a, R.A. Manzoni^{a,b}, B. Marzocchi^{a,b,2}, D. Menasce^a, L. Moroni^a, M. Paganoni^{a,b}, D. Pedrini^a, S. Ragazzi^{a,b}, N. Redaelli^a, T. Tabarelli de Fatis^{a,b}

INFN Sezione di Napoli^a, Università di Napoli 'Federico II'^b, Napoli, Italy, Università della Basilicata^c, Potenza, Italy, Università G. Marconi^d, Roma, Italy

S. Buontempo^a, N. Cavallo^{a,c}, S. Di Guida^{a,d,2}, M. Esposito^{a,b}, F. Fabozzi^{a,c}, A.O.M. Iorio^{a,b}, G. Lanza^a, L. Lista^a, S. Meola^{a,d,2}, M. Merola^a, P. Paolucci^{a,2}, C. Sciacca^{a,b}, F. Thyssen

INFN Sezione di Padova^a, Università di Padova^b, Padova, Italy, Università di Trento^c, Trento, Italy

P. Azzi^{a,2}, N. Bacchetta^a, L. Benato^{a,b}, D. Bisello^{a,b}, A. Boletti^{a,b}, R. Carlin^{a,b}, P. Checchia^a, M. Dall'Osso^{a,b,2}, T. Dorigo^a, F. Gasparini^{a,b}, U. Gasparini^{a,b}, A. Gozzelino^a, K. Kanishchev^{a,c}, S. Lacaprara^a, M. Margoni^{a,b}, A.T. Meneguzzo^{a,b}, J. Pazzini^{a,b}, M. Pegoraro^a, N. Pozzobon^{a,b}, P. Ronchese^{a,b}, F. Simonetto^{a,b}, E. Torassa^a, M. Tosi^{a,b}, S. Vanini^{a,b}, S. Ventura^a, M. Zanetti, P. Zotto^{a,b}, A. Zucchetta^{a,b,2}, G. Zumerle^{a,b}

INFN Sezione di Pavia^a, Università di Pavia^b, Pavia, Italy

A. Braghieri^a, A. Magnani^a, P. Montagna^{a,b}, S.P. Ratti^{a,b}, V. Re^a, C. Riccardi^{a,b}, P. Salvini^a, I. Vai^a, P. Vitulo^{a,b}

INFN Sezione di Perugia^a, Università di Perugia^b, Perugia, Italy

L. Alunni Solestizi^{a,b}, M. Biasini^{a,b}, G.M. Bilei^a, D. Ciangottini^{a,b,2}, L. Fanò^{a,b}, P. Lariccia^{a,b}, G. Mantovani^{a,b}, M. Menichelli^a, A. Saha^a, A. Santocchia^{a,b}, A. Spiezia^{a,b}

INFN Sezione di Pisa^a, Università di Pisa^b, Scuola Normale Superiore di Pisa^c, Pisa, Italy

K. Androsov^{a,31}, P. Azzurri^a, G. Bagliesi^a, J. Bernardini^a, T. Boccali^a, G. Broccolo^{a,c}, R. Castaldi^a, M.A. Ciocci^{a,31}, R. Dell'Orso^a, S. Donato^{a,c,2}, G. Fedi, L. Foà^{a,c†}, A. Giassi^a, M.T. Grippo^{a,31}, F. Ligabue^{a,c}, T. Lomtadze^a, L. Martini^{a,b}, A. Messineo^{a,b}, F. Palla^a, A. Rizzi^{a,b}, A. Savoy-Navarro^{a,32}, A.T. Serban^a, P. Spagnolo^a, P. Squillacioti^{a,31}, R. Tenchini^a, G. Tonelli^{a,b}, A. Venturi^a, P.G. Verdini^a

INFN Sezione di Roma^a, Università di Roma^b, Roma, Italy

L. Barone^{a,b}, F. Cavallari^a, G. D'imperio^{a,b,2}, D. Del Re^{a,b}, M. Diemoz^a, S. Gelli^{a,b}, C. Jorda^a, E. Longo^{a,b}, F. Margaroli^{a,b}, P. Meridiani^a, G. Organtini^{a,b}, R. Paramatti^a, F. Preiato^{a,b}, S. Rahatlou^{a,b}, C. Rovelli^a, F. Santanastasio^{a,b}, P. Traczyk^{a,b,2}

INFN Sezione di Torino^a, Università di Torino^b, Torino, Italy, Università del Piemonte Orientale^c, Novara, Italy

N. Amapane^{a,b}, R. Arcidiacono^{a,c,2}, S. Argiro^{a,b}, M. Arneodo^{a,c}, R. Bellan^{a,b}, C. Biino^a, N. Cartiglia^a, M. Costa^{a,b}, R. Covarelli^{a,b}, A. Degano^{a,b}, N. Demaria^a, L. Finco^{a,b,2}, B. Kiani^{a,b}, C. Mariotti^a, S. Maselli^a, G. Mazza^a, E. Migliore^{a,b}, V. Monaco^{a,b}, E. Monteil^{a,b}, M. Musich^a, M.M. Obertino^{a,b}, L. Pacher^{a,b}, N. Pastrone^a, M. Pelliccioni^a, G.L. Pinna Angioni^{a,b}, F. Ravera^{a,b}, A. Romero^{a,b}, M. Ruspa^{a,c}, R. Sacchi^{a,b}, A. Solano^{a,b}, A. Staiano^a

INFN Sezione di Trieste^a, Università di Trieste^b, Trieste, Italy

S. Belforte^a, V. Candelise^{a,b,2}, M. Casarsa^a, F. Cossutti^a, G. Della Ricca^{a,b}, B. Gobbo^a, C. La Licata^{a,b}, M. Marone^{a,b}, A. Schizzi^{a,b}, A. Zanetti^a

Kangwon National University, Chunchon, Korea

A. Kropivnitskaya, S.K. Nam

Kyungpook National University, Daegu, Korea

D.H. Kim, G.N. Kim, M.S. Kim, D.J. Kong, S. Lee, Y.D. Oh, A. Sakharov, D.C. Son

Chonbuk National University, Jeonju, Korea

J.A. Brochero Cifuentes, H. Kim, T.J. Kim, M.S. Ryu

Chonnam National University, Institute for Universe and Elementary Particles, Kwangju, Korea

S. Song

Korea University, Seoul, Korea

S. Choi, Y. Go, D. Gyun, B. Hong, M. Jo, H. Kim, Y. Kim, B. Lee, K. Lee, K.S. Lee, S. Lee, S.K. Park, Y. Roh

Seoul National University, Seoul, Korea

H.D. Yoo

University of Seoul, Seoul, Korea

M. Choi, H. Kim, J.H. Kim, J.S.H. Lee, I.C. Park, G. Ryu

Sungkyunkwan University, Suwon, Korea

Y. Choi, J. Goh, D. Kim, E. Kwon, J. Lee, I. Yu

Vilnius University, Vilnius, Lithuania

A. Juodagalvis, J. Vaitkus

National Centre for Particle Physics, Universiti Malaya, Kuala Lumpur, Malaysia

I. Ahmed, Z.A. Ibrahim, J.R. Komaragiri, M.A.B. Md Ali³³, F. Mohamad Idris³⁴, W.A.T. Wan Abdullah, M.N. Yusli

Centro de Investigacion y de Estudios Avanzados del IPN, Mexico City, Mexico

E. Casimiro Linares, H. Castilla-Valdez, E. De La Cruz-Burelo, I. Heredia-de La Cruz³⁵, A. Hernandez-Almada, R. Lopez-Fernandez, A. Sanchez-Hernandez

Universidad Iberoamericana, Mexico City, Mexico

S. Carrillo Moreno, F. Vazquez Valencia

Benemerita Universidad Autonoma de Puebla, Puebla, Mexico

I. Pedraza, H.A. Salazar Ibarguen

Universidad Autónoma de San Luis Potosí, San Luis Potosí, Mexico

A. Morelos Pineda

University of Auckland, Auckland, New Zealand

D. Krofcheck

University of Canterbury, Christchurch, New Zealand

P.H. Butler

National Centre for Physics, Quaid-I-Azam University, Islamabad, Pakistan

A. Ahmad, M. Ahmad, Q. Hassan, H.R. Hoorani, W.A. Khan, T. Khurshid, M. Shoaib

National Centre for Nuclear Research, Swierk, Poland

H. Bialkowska, M. Bluj, B. Boimska, T. Frueboes, M. Górski, M. Kazana, K. Nawrocki, K. Romanowska-Rybinska, M. Szleper, P. Zalewski

Institute of Experimental Physics, Faculty of Physics, University of Warsaw, Warsaw, Poland

G. Brona, K. Bunkowski, A. Byszuk³⁶, K. Doroba, A. Kalinowski, M. Konecki, J. Krolikowski, M. Misiura, M. Olszewski, M. Walczak

Laboratório de Instrumentação e Física Experimental de Partículas, Lisboa, Portugal

P. Bargassa, C. Beirão Da Cruz E Silva, A. Di Francesco, P. Faccioli, P.G. Ferreira Parracho, M. Gallinaro, N. Leonardo, L. Lloret Iglesias, F. Nguyen, J. Rodrigues Antunes, J. Seixas, O. Toldaiev, D. Vadrucio, J. Varela, P. Vischia

Joint Institute for Nuclear Research, Dubna, Russia

S. Afanasiev, P. Bunin, M. Gavrilenko, I. Golutvin, I. Gorbunov, A. Kamenev, V. Karjavin, V. Konoplyanikov, A. Lanev, A. Malakhov, V. Matveev³⁷, P. Moiseenz, V. Palichik, V. Perelygin, S. Shmatov, S. Shulha, N. Skatchkov, V. Smirnov, A. Zarubin

Petersburg Nuclear Physics Institute, Gatchina (St. Petersburg), Russia

V. Golovtsov, Y. Ivanov, V. Kim³⁸, E. Kuznetsova, P. Levchenko, V. Murzin, V. Oreshkin, I. Smirnov, V. Sulimov, L. Uvarov, S. Vavilov, A. Vorobyev

Institute for Nuclear Research, Moscow, Russia

Yu. Andreev, A. Dermenev, S. Gninenko, N. Golubev, A. Karneyeu, M. Kirsanov, N. Krasnikov, A. Pashenkov, D. Tlisov, A. Toropin

Institute for Theoretical and Experimental Physics, Moscow, Russia

V. Epshteyn, V. Gavrillov, N. Lychkovskaya, V. Popov, I. Pozdnyakov, G. Safronov, A. Spiridonov, E. Vlasov, A. Zhokin

National Research Nuclear University 'Moscow Engineering Physics Institute' (MEPhI), Moscow, Russia

A. Bylinkin

P.N. Lebedev Physical Institute, Moscow, Russia

V. Andreev, M. Azarkin³⁹, I. Dremin³⁹, M. Kirakosyan, A. Leonidov³⁹, G. Mesyats, S.V. Rusakov, A. Vinogradov

Skobeltsyn Institute of Nuclear Physics, Lomonosov Moscow State University, Moscow, Russia

A. Baskakov, A. Belyaev, E. Boos, V. Bunichev, M. Dubinin⁴⁰, L. Dudko, A. Gribushin, V. Klyukhin, O. Kodolova, N. Korneeva, I. Lokhtin, I. Myagkov, S. Obraztsov, M. Perfilov, V. Savrin

State Research Center of Russian Federation, Institute for High Energy Physics, Protvino, Russia

I. Azhgirey, I. Bayshev, S. Bitioukov, V. Kachanov, A. Kalinin, D. Konstantinov, V. Krychkin, V. Petrov, R. Ryutin, A. Sobol, L. Tourtchanovitch, S. Troshin, N. Tyurin, A. Uzunian, A. Volkov

University of Belgrade, Faculty of Physics and Vinca Institute of Nuclear Sciences, Belgrade, Serbia

P. Adzic⁴¹, M. Ekmedzic, J. Milosevic, V. Rekovic

Centro de Investigaciones Energéticas Medioambientales y Tecnológicas (CIEMAT), Madrid, Spain

J. Alcaraz Maestre, E. Calvo, M. Cerrada, M. Chamizo Llatas, N. Colino, B. De La Cruz, A. Delgado Peris, D. Domínguez Vázquez, A. Escalante Del Valle, C. Fernandez Bedoya, J.P. Fernández Ramos, J. Flix, M.C. Fouz, P. Garcia-Abia, O. Gonzalez Lopez, S. Goy Lopez, J.M. Hernandez, M.I. Josa, E. Navarro De Martino, A. Pérez-Calero Yzquierdo, J. Puerta Pelayo, A. Quintario Olmeda, I. Redondo, L. Romero, J. Santaolalla, M.S. Soares

Universidad Autónoma de Madrid, Madrid, Spain

C. Albajar, J.F. de Trocóniz, M. Missiroli, D. Moran

Universidad de Oviedo, Oviedo, Spain

J. Cuevas, J. Fernandez Menendez, S. Folgueras, I. Gonzalez Caballero, E. Palencia Cortezon, J.M. Vizan Garcia

Instituto de Física de Cantabria (IFCA), CSIC-Universidad de Cantabria, Santander, Spain

I.J. Cabrillo, A. Calderon, J.R. Castiñeiras De Saa, P. De Castro Manzano, J. Duarte Campderros, M. Fernandez, J. Garcia-Ferrero, G. Gomez, A. Lopez Virto, J. Marco, R. Marco, C. Martinez Rivero, F. Matorras, F.J. Munoz Sanchez, J. Piedra Gomez, T. Rodrigo, A.Y. Rodríguez-Marrero, A. Ruiz-Jimeno, L. Scodellaro, I. Vila, R. Vilar Cortabitarte

CERN, European Organization for Nuclear Research, Geneva, Switzerland

D. Abbaneo, E. Auffray, G. Auzinger, M. Bachtis, P. Baillon, A.H. Ball, D. Barney, A. Benaglia, J. Bendavid, L. Benhabib, J.F. Benitez, G.M. Berruti, P. Bloch, A. Bocci, A. Bonato, C. Botta, H. Breuker, T. Camporesi, R. Castello, G. Cerminara, S. Colafranceschi⁴², M. D'Alfonso, D. d'Enterria, A. Dabrowski, V. Daponte, A. David, M. De Gruttola, F. De Guio, A. De Roeck, S. De Visscher, E. Di Marco, M. Dobson, M. Dordevic, B. Dorney, T. du Pree, M. Dünser, N. Dupont, A. Elliott-Peisert, G. Franzoni, W. Funk, D. Gigi, K. Gill, D. Giordano, M. Girone, F. Glege, R. Guida, S. Gundacker, M. Guthoff, J. Hammer, P. Harris, J. Hegeman, V. Innocente, P. Janot, H. Kirschenmann, M.J. Kortelainen, K. Kousouris, K. Krajczar, P. Lecoq, C. Lourenço, M.T. Lucchini, N. Magini, L. Malgeri, M. Mannelli, A. Martelli, L. Masetti, F. Meijers, S. Mersi, E. Meschi, F. Moortgat, S. Morovic, M. Mulders, M.V. Nemallapudi, H. Neugebauer, S. Orfanelli⁴³, L. Orsini, L. Pape, E. Perez, M. Peruzzi, A. Petrilli, G. Petrucciani, A. Pfeiffer, D. Piparo, A. Racz, G. Rolandi⁴⁴, M. Rovere, M. Ruan, H. Sakulin, C. Schäfer, C. Schwick, A. Sharma, P. Silva, M. Simon, P. Sphicas⁴⁵, D. Spiga, J. Steggemann, B. Stieger, M. Stoye, Y. Takahashi, D. Treille, A. Triossi, A. Tsirou, G.I. Veres²², N. Wardle, H.K. Wöhri, A. Zagodzinska³⁶, W.D. Zeuner

Paul Scherrer Institut, Villigen, Switzerland

W. Bertl, K. Deiters, W. Erdmann, R. Horisberger, Q. Ingram, H.C. Kaestli, D. Kotlinski, U. Langenegger, D. Renker, T. Rohe

Institute for Particle Physics, ETH Zurich, Zurich, Switzerland

F. Bachmair, L. Bäni, L. Bianchini, M.A. Buchmann, B. Casal, G. Dissertori, M. Dittmar, M. Donegà, P. Eller, C. Grab, C. Heidegger, D. Hits, J. Hoss, G. Kasieczka, W. Lustermann, B. Mangano, M. Marionneau, P. Martinez Ruiz del Arbol, M. Masciovecchio, D. Meister, F. Micheli, P. Musella, F. Nessi-Tedaldi, F. Pandolfi, J. Pata, F. Pauss, L. Perrozzi, M. Quitnat, M. Rossini, A. Starodumov⁴⁶, M. Takahashi, V.R. Tavolaro, K. Theofilatos, R. Wallny

Universität Zürich, Zurich, Switzerland

T.K. Aarrestad, C. AMSler⁴⁷, L. Caminada, M.F. Canelli, V. Chiochia, A. De Cosa, C. Galloni, A. Hinzmann, T. Hreus, B. Kilminster, C. Lange, J. Ngadiuba, D. Pinna, P. Robmann, F.J. Ronga, D. Salerno, Y. Yang

National Central University, Chung-Li, Taiwan

M. Cardaci, K.H. Chen, T.H. Doan, Sh. Jain, R. Khurana, M. Konyushikhin, C.M. Kuo, W. Lin, Y.J. Lu, S.S. Yu

National Taiwan University (NTU), Taipei, Taiwan

Arun Kumar, R. Bartek, P. Chang, Y.H. Chang, Y.W. Chang, Y. Chao, K.F. Chen, P.H. Chen, C. Dietz, F. Fiori, U. Grundler, W.-S. Hou, Y. Hsiung, Y.F. Liu, R.-S. Lu, M. Miñano Moya, E. Petrakou, J.f. Tsai, Y.M. Tzeng

Chulalongkorn University, Faculty of Science, Department of Physics, Bangkok, Thailand

B. Asavapibhop, K. Kovitanggoon, G. Singh, N. Srimanobhas, N. Suwonjandee

Cukurova University, Adana, Turkey

A. Adiguzel, M.N. Bakirci⁴⁸, S. Cerci⁴⁹, Z.S. Demiroglu, C. Dozen, I. Dumanoglu, E. Eskut, S. Girgis, G. Gokbulut, Y. Guler, E. Gurpinar, I. Hos, E.E. Kangal⁵⁰, G. Onengut⁵¹, K. Ozdemir⁵², A. Polatoz, D. Sunar Cerci⁴⁹, M. Vergili, C. Zorbilmez

Middle East Technical University, Physics Department, Ankara, Turkey

I.V. Akin, B. Bilin, S. Bilmis, B. Isildak⁵³, G. Karapinar⁵⁴, M. Yalvac, M. Zeyrek

Bogazici University, Istanbul, Turkey

E.A. Albayrak⁵⁵, E. Gülmez, M. Kaya⁵⁶, O. Kaya⁵⁷, T. Yetkin⁵⁸

Istanbul Technical University, Istanbul, Turkey

K. Cankocak, S. Sen⁵⁹, F.I. Vardarli

Institute for Scintillation Materials of National Academy of Science of Ukraine, Kharkov, Ukraine

B. Grynyov

National Scientific Center, Kharkov Institute of Physics and Technology, Kharkov, Ukraine

L. Levchuk, P. Sorokin

University of Bristol, Bristol, United Kingdom

R. Aggleton, F. Ball, L. Beck, J.J. Brooke, E. Clement, D. Cussans, H. Flacher, J. Goldstein, M. Grimes, G.P. Heath, H.F. Heath, J. Jacob, L. Kreczko, C. Lucas, Z. Meng, D.M. Newbold⁶⁰, S. Paramesvaran, A. Poll, T. Sakuma, S. Seif El Nasr-storey, S. Senkin, D. Smith, V.J. Smith

Rutherford Appleton Laboratory, Didcot, United Kingdom

K.W. Bell, A. Belyaev⁶¹, C. Brew, R.M. Brown, D. Cieri, D.J.A. Cockerill, J.A. Coughlan, K. Harder, S. Harper, E. Olaiya, D. Petyt, C.H. Shepherd-Themistocleous, A. Thea, I.R. Tomalin, T. Williams, W.J. Womersley, S.D. Worm

Imperial College, London, United Kingdom

M. Baber, R. Bainbridge, O. Buchmuller, A. Bundock, D. Burton, S. Casasso, M. Citron, D. Colling, L. Corpe, N. Cripps, P. Dauncey, G. Davies, A. De Wit, M. Della Negra, P. Dunne, A. Elwood, W. Ferguson, J. Fulcher, D. Futyan, G. Hall, G. Iles, M. Kenzie, R. Lane, R. Lucas⁶⁰, L. Lyons, A.-M. Magnan, S. Malik, J. Nash, A. Nikitenko⁴⁶, J. Pela, M. Pesaresi, K. Petridis, D.M. Raymond, A. Richards, A. Rose, C. Seez, A. Tapper, K. Uchida, M. Vazquez Acosta⁶², T. Virdee, S.C. Zenz

Brunel University, Uxbridge, United Kingdom

J.E. Cole, P.R. Hobson, A. Khan, P. Kyberd, D. Leggat, D. Leslie, I.D. Reid, P. Symonds, L. Teodorescu, M. Turner

Baylor University, Waco, USA

A. Borzou, K. Call, J. Dittmann, K. Hatakeyama, A. Kasmi, H. Liu, N. Pastika

The University of Alabama, Tuscaloosa, USA

O. Charaf, S.I. Cooper, C. Henderson, P. Rumerio

Boston University, Boston, USA

A. Avetisyan, T. Bose, C. Fantasia, D. Gastler, P. Lawson, D. Rankin, C. Richardson, J. Rohlf, J. St. John, L. Sulak, D. Zou

Brown University, Providence, USA

J. Alimena, E. Berry, S. Bhattacharya, D. Cutts, N. Dhingra, A. Ferapontov, A. Garabedian, J. Hakala, U. Heintz, E. Laird, G. Landsberg, Z. Mao, M. Narain, S. Piperov, S. Sagir, T. Sinthuprasith, R. Syarif

University of California, Davis, Davis, USA

R. Breedon, G. Breto, M. Calderon De La Barca Sanchez, S. Chauhan, M. Chertok, J. Conway, R. Conway, P.T. Cox, R. Erbacher, M. Gardner, W. Ko, R. Lander, M. Mulhearn, D. Pellett, J. Pilot, F. Ricci-Tam, S. Shalhout, J. Smith, M. Squires, D. Stolp, M. Tripathi, S. Wilbur, R. Yohay

University of California, Los Angeles, USA

R. Cousins, P. Everaerts, C. Farrell, J. Hauser, M. Ignatenko, D. Saltzberg, E. Takasugi, V. Valuev, M. Weber

University of California, Riverside, Riverside, USA

K. Burt, R. Clare, J. Ellison, J.W. Gary, G. Hanson, J. Heilman, M. Ivova PANEVA, P. Jandir, E. Kennedy, F. Lacroix, O.R. Long, A. Luthra, M. Malberti, M. Olmedo Negrete, A. Shrinivas, H. Wei, S. Wimpenny, B. R. Yates

University of California, San Diego, La Jolla, USA

J.G. Branson, G.B. Cerati, S. Cittolin, R.T. D'Agnolo, A. Holzner, R. Kelley, D. Klein, J. Letts, I. Macneill, D. Olivito, S. Padhi, M. Pieri, M. Sani, V. Sharma, S. Simon, M. Tadel, A. Vartak, S. Wasserbaech⁶³, C. Welke, F. Würthwein, A. Yagil, G. Zevi Della Porta

University of California, Santa Barbara, Santa Barbara, USA

D. Barge, J. Bradmiller-Feld, C. Campagnari, A. Dishaw, V. Dutta, K. Flowers, M. Franco Sevilla, P. Geffert, C. George, F. Golf, L. Gouskos, J. Gran, J. Incandela, C. Justus, N. Mccoll, S.D. Mullin, J. Richman, D. Stuart, I. Suarez, W. To, C. West, J. Yoo

California Institute of Technology, Pasadena, USA

D. Anderson, A. Apresyan, A. Bornheim, J. Bunn, Y. Chen, J. Duarte, A. Mott, H.B. Newman, C. Pena, M. Pierini, M. Spiropulu, J.R. Vlimant, S. Xie, R.Y. Zhu

Carnegie Mellon University, Pittsburgh, USA

M.B. Andrews, V. Azzolini, A. Calamba, B. Carlson, T. Ferguson, M. Paulini, J. Russ, M. Sun, H. Vogel, I. Vorobiev

University of Colorado Boulder, Boulder, USA

J.P. Cumalat, W.T. Ford, A. Gaz, F. Jensen, A. Johnson, M. Krohn, T. Mulholland, U. Nauenberg, K. Stenson, S.R. Wagner

Cornell University, Ithaca, USA

J. Alexander, A. Chatterjee, J. Chaves, J. Chu, S. Dittmer, N. Eggert, N. Mirman, G. Nicolas Kaufman, J.R. Patterson, A. Rinkevicius, A. Ryd, L. Skinnari, L. Soffi, W. Sun, S.M. Tan, W.D. Teo, J. Thom, J. Thompson, J. Tucker, Y. Weng, P. Wittich

Fermi National Accelerator Laboratory, Batavia, USA

S. Abdullin, M. Albrow, J. Anderson, G. Apollinari, S. Banerjee, L.A.T. Bauerdick, A. Beretvas, J. Berryhill, P.C. Bhat, G. Bolla, K. Burkett, J.N. Butler, H.W.K. Cheung, F. Chlebana, S. Cihangir, V.D. Elvira, I. Fisk, J. Freeman, E. Gottschalk, L. Gray, D. Green, S. Grünendahl, O. Gutsche, J. Hanlon, D. Hare, R.M. Harris, S. Hasegawa, J. Hirschauer, Z. Hu, S. Jindariani, M. Johnson, U. Joshi, A.W. Jung, B. Klima, B. Kreis, S. Kwan[†], S. Lammel, J. Linacre, D. Lincoln, R. Lipton, T. Liu, R. Lopes De Sá, J. Lykken, K. Maeshima, J.M. Marraffino, V.I. Martinez Outschoorn,

S. Maruyama, D. Mason, P. McBride, P. Merkel, K. Mishra, S. Mrenna, S. Nahn, C. Newman-Holmes, V. O'Dell, K. Pedro, O. Prokofyev, G. Rakness, E. Sexton-Kennedy, A. Soha, W.J. Spalding, L. Spiegel, L. Taylor, S. Tkaczyk, N.V. Tran, L. Uplegger, E.W. Vaandering, C. Vernieri, M. Verzocchi, R. Vidal, H.A. Weber, A. Whitbeck, F. Yang

University of Florida, Gainesville, USA

D. Acosta, P. Avery, P. Bortignon, D. Bourilkov, A. Carnes, M. Carver, D. Curry, S. Das, G.P. Di Giovanni, R.D. Field, I.K. Furic, J. Hugon, J. Konigsberg, A. Korytov, J.F. Low, P. Ma, K. Matchev, H. Mei, P. Milenovic⁶⁴, G. Mitselmakher, D. Rank, R. Rossin, L. Shchutska, M. Snowball, D. Sperka, N. Terentyev, L. Thomas, J. Wang, S. Wang, J. Yelton

Florida International University, Miami, USA

S. Hewamanage, S. Linn, P. Markowitz, G. Martinez, J.L. Rodriguez

Florida State University, Tallahassee, USA

A. Ackert, J.R. Adams, T. Adams, A. Askew, J. Bochenek, B. Diamond, J. Haas, S. Hagopian, V. Hagopian, K.F. Johnson, A. Khatiwada, H. Prosper, M. Weinberg

Florida Institute of Technology, Melbourne, USA

M.M. Baarmand, V. Bhopatkar, M. Hohlmann, H. Kalakhety, D. Noonan, T. Roy, F. Yumiceva

University of Illinois at Chicago (UIC), Chicago, USA

M.R. Adams, L. Apanasevich, D. Berry, R.R. Betts, I. Bucinskaite, R. Cavanaugh, O. Evdokimov, L. Gauthier, C.E. Gerber, D.J. Hofman, P. Kurt, C. O'Brien, I.D. Sandoval Gonzalez, C. Silkworth, P. Turner, N. Varelas, Z. Wu, M. Zakaria

The University of Iowa, Iowa City, USA

B. Bilki⁶⁵, W. Clarida, K. Dilsiz, S. Durgut, R.P. Gandrajula, M. Haytmyradov, V. Khristenko, J.-P. Merlo, H. Mermerkaya⁶⁶, A. Mestvirishvili, A. Moeller, J. Nachtman, H. Ogul, Y. Onel, F. Ozok⁶⁷, A. Penzo, C. Snyder, P. Tan, E. Tiras, J. Wetzel, K. Yi

Johns Hopkins University, Baltimore, USA

I. Anderson, B.A. Barnett, B. Blumenfeld, D. Fehling, L. Feng, A.V. Gritsan, P. Maksimovic, C. Martin, M. Osherson, M. Swartz, M. Xiao, Y. Xin, C. You

The University of Kansas, Lawrence, USA

P. Baringer, A. Bean, G. Benelli, C. Bruner, R.P. Kenny III, D. Majumder, M. Malek, M. Murray, S. Sanders, R. Stringer, Q. Wang

Kansas State University, Manhattan, USA

A. Ivanov, K. Kaadze, S. Khalil, M. Makouski, Y. Maravin, A. Mohammadi, L.K. Saini, N. Skhirtladze, S. Toda

Lawrence Livermore National Laboratory, Livermore, USA

D. Lange, F. Rebassoo, D. Wright

University of Maryland, College Park, USA

C. Anelli, A. Baden, O. Baron, A. Belloni, B. Calvert, S.C. Eno, C. Ferraioli, J.A. Gomez, N.J. Hadley, S. Jabeen, R.G. Kellogg, T. Kolberg, J. Kunkle, Y. Lu, A.C. Mignerey, Y.H. Shin, A. Skuja, M.B. Tonjes, S.C. Tonwar

Massachusetts Institute of Technology, Cambridge, USA

A. Apyan, R. Barbieri, A. Baty, K. Bierwagen, S. Brandt, W. Busza, I.A. Cali, Z. Demiragli, L. Di Matteo, G. Gomez Ceballos, M. Goncharov, D. Gulhan, Y. Iiyama, G.M. Innocenti, M. Klute, D. Kovalskyi, Y.S. Lai, Y.-J. Lee, A. Levin, P.D. Luckey, A.C. Marini, C. Mcginn,

C. Mironov, X. Niu, C. Paus, D. Ralph, C. Roland, G. Roland, J. Salfeld-Nebgen, G.S.F. Stephans, K. Sumorok, M. Varma, D. Velicanu, J. Veverka, J. Wang, T.W. Wang, B. Wyslouch, M. Yang, V. Zhukova

University of Minnesota, Minneapolis, USA

B. Dahmes, A. Evans, A. Finkel, A. Gude, P. Hansen, S. Kalafut, S.C. Kao, K. Klapoetke, Y. Kubota, Z. Lesko, J. Mans, S. Nourbakhsh, N. Ruckstuhl, R. Rusack, N. Tambe, J. Turkewitz

University of Mississippi, Oxford, USA

J.G. Acosta, S. Oliveros

University of Nebraska-Lincoln, Lincoln, USA

E. Avdeeva, K. Bloom, S. Bose, D.R. Claes, A. Dominguez, C. Fangmeier, R. Gonzalez Suarez, R. Kamalieddin, J. Keller, D. Knowlton, I. Kravchenko, J. Lazo-Flores, F. Meier, J. Monroy, F. Ratnikov, J.E. Siado, G.R. Snow

State University of New York at Buffalo, Buffalo, USA

M. Alyari, J. Dolen, J. George, A. Godshalk, C. Harrington, I. Iashvili, J. Kaisen, A. Kharchilava, A. Kumar, S. Rappoccio

Northeastern University, Boston, USA

G. Alverson, E. Barberis, D. Baumgartel, M. Chasco, A. Hortiangtham, A. Massironi, D.M. Morse, D. Nash, T. Orimoto, R. Teixeira De Lima, D. Trocino, R.-J. Wang, D. Wood, J. Zhang

Northwestern University, Evanston, USA

K.A. Hahn, A. Kubik, N. Mucia, N. Odell, B. Pollack, A. Pozdnyakov, M. Schmitt, S. Stoynev, K. Sung, M. Trovato, M. Velasco

University of Notre Dame, Notre Dame, USA

A. Brinkerhoff, N. Dev, M. Hildreth, C. Jessop, D.J. Karmgard, N. Kellams, K. Lannon, S. Lynch, N. Marinelli, F. Meng, C. Mueller, Y. Musienko³⁷, T. Pearson, M. Planer, A. Reinsvold, R. Ruchti, G. Smith, S. Taroni, N. Valls, M. Wayne, M. Wolf, A. Woodard

The Ohio State University, Columbus, USA

L. Antonelli, J. Brinson, B. Bylsma, L.S. Durkin, S. Flowers, A. Hart, C. Hill, R. Hughes, W. Ji, K. Kotov, T.Y. Ling, B. Liu, W. Luo, D. Puigh, M. Rodenburg, B.L. Winer, H.W. Wulsin

Princeton University, Princeton, USA

O. Driga, P. Elmer, J. Hardenbrook, P. Hebda, S.A. Koay, P. Lujan, D. Marlow, T. Medvedeva, M. Mooney, J. Olsen, C. Palmer, P. Piroué, X. Quan, H. Saka, D. Stickland, C. Tully, J.S. Werner, A. Zuranski

University of Puerto Rico, Mayaguez, USA

S. Malik

Purdue University, West Lafayette, USA

V.E. Barnes, D. Benedetti, D. Bortoletto, L. Gutay, M.K. Jha, M. Jones, K. Jung, D.H. Miller, N. Neumeister, B.C. Radburn-Smith, X. Shi, I. Shipsey, D. Silvers, J. Sun, A. Svyatkovskiy, F. Wang, W. Xie, L. Xu

Purdue University Calumet, Hammond, USA

N. Parashar, J. Stupak

Rice University, Houston, USA

A. Adair, B. Akgun, Z. Chen, K.M. Ecklund, F.J.M. Geurts, M. Guilbaud, W. Li, B. Michlin, M. Northup, B.P. Padley, R. Redjimi, J. Roberts, J. Rorie, Z. Tu, J. Zabel

University of Rochester, Rochester, USA

B. Betchart, A. Bodek, P. de Barbaro, R. Demina, Y. Eshaq, T. Ferbel, M. Galanti, A. Garcia-Bellido, J. Han, A. Harel, O. Hindrichs, A. Khukhunaishvili, G. Petrillo, M. Verzetti

The Rockefeller University, New York, USA

L. Demortier

Rutgers, The State University of New Jersey, Piscataway, USA

S. Arora, A. Barker, J.P. Chou, C. Contreras-Campana, E. Contreras-Campana, D. Duggan, D. Ferencek, Y. Gershtein, R. Gray, E. Halkiadakis, D. Hidas, E. Hughes, S. Kaplan, R. Kunnawalkam Elayavalli, A. Lath, K. Nash, S. Panwalkar, M. Park, S. Salur, S. Schnetzer, D. Sheffield, S. Somalwar, R. Stone, S. Thomas, P. Thomassen, M. Walker

University of Tennessee, Knoxville, USA

M. Foerster, G. Riley, K. Rose, S. Spanier, A. York

Texas A&M University, College Station, USA

O. Bouhali⁶⁸, A. Castaneda Hernandez⁶⁸, M. Dalchenko, M. De Mattia, A. Delgado, S. Dildick, R. Eusebi, W. Flanagan, J. Gilmore, T. Kamon⁶⁹, V. Krutelyov, R. Mueller, I. Osipenkov, Y. Pakhotin, R. Patel, A. Perloff, A. Rose, A. Safonov, A. Tatarinov, K.A. Ulmer²

Texas Tech University, Lubbock, USA

N. Akchurin, C. Cowden, J. Damgov, C. Dragoiu, P.R. Duerdo, J. Faulkner, S. Kunori, K. Lamichhane, S.W. Lee, T. Libeiro, S. Undleeb, I. Volobouev

Vanderbilt University, Nashville, USA

E. Appelt, A.G. Delannoy, S. Greene, A. Gurrola, R. Janjam, W. Johns, C. Maguire, Y. Mao, A. Melo, H. Ni, P. Sheldon, B. Snook, S. Tuo, J. Velkovska, Q. Xu

University of Virginia, Charlottesville, USA

M.W. Arenton, S. Boutle, B. Cox, B. Francis, J. Goodell, R. Hirosky, A. Ledovskoy, H. Li, C. Lin, C. Neu, X. Sun, Y. Wang, E. Wolfe, J. Wood, F. Xia

Wayne State University, Detroit, USA

C. Clarke, R. Harr, P.E. Karchin, C. Kottachchi Kankanamge Don, P. Lamichhane, J. Sturdy

University of Wisconsin, Madison, USA

D.A. Belknap, D. Carlsmith, M. Cepeda, A. Christian, S. Dasu, L. Dodd, S. Duric, E. Friis, B. Gomber, M. Grothe, R. Hall-Wilton, M. Herndon, A. Hervé, P. Klabbbers, A. Lanaro, A. Levine, K. Long, R. Loveless, A. Mohapatra, I. Ojalvo, T. Perry, G.A. Pierro, G. Polese, T. Ruggles, T. Sarangi, A. Savin, A. Sharma, N. Smith, W.H. Smith, D. Taylor, N. Woods

†: Deceased

1: Also at Vienna University of Technology, Vienna, Austria

2: Also at CERN, European Organization for Nuclear Research, Geneva, Switzerland

3: Also at State Key Laboratory of Nuclear Physics and Technology, Peking University, Beijing, China

4: Also at Institut Pluridisciplinaire Hubert Curien, Université de Strasbourg, Université de Haute Alsace Mulhouse, CNRS/IN2P3, Strasbourg, France

5: Also at National Institute of Chemical Physics and Biophysics, Tallinn, Estonia

6: Also at Skobeltsyn Institute of Nuclear Physics, Lomonosov Moscow State University,

Moscow, Russia

- 7: Also at Universidade Estadual de Campinas, Campinas, Brazil
- 8: Also at Centre National de la Recherche Scientifique (CNRS) - IN2P3, Paris, France
- 9: Also at Laboratoire Leprince-Ringuet, Ecole Polytechnique, IN2P3-CNRS, Palaiseau, France
- 10: Also at Joint Institute for Nuclear Research, Dubna, Russia
- 11: Also at Helwan University, Cairo, Egypt
- 12: Now at Zewail City of Science and Technology, Zewail, Egypt
- 13: Also at Ain Shams University, Cairo, Egypt
- 14: Now at British University in Egypt, Cairo, Egypt
- 15: Also at Fayoum University, El-Fayoum, Egypt
- 16: Also at Université de Haute Alsace, Mulhouse, France
- 17: Also at Tbilisi State University, Tbilisi, Georgia
- 18: Also at RWTH Aachen University, III. Physikalisches Institut A, Aachen, Germany
- 19: Also at University of Hamburg, Hamburg, Germany
- 20: Also at Brandenburg University of Technology, Cottbus, Germany
- 21: Also at Institute of Nuclear Research ATOMKI, Debrecen, Hungary
- 22: Also at Eötvös Loránd University, Budapest, Hungary
- 23: Also at University of Debrecen, Debrecen, Hungary
- 24: Also at Wigner Research Centre for Physics, Budapest, Hungary
- 25: Also at University of Visva-Bharati, Santiniketan, India
- 26: Now at King Abdulaziz University, Jeddah, Saudi Arabia
- 27: Also at University of Ruhuna, Matara, Sri Lanka
- 28: Also at Isfahan University of Technology, Isfahan, Iran
- 29: Also at University of Tehran, Department of Engineering Science, Tehran, Iran
- 30: Also at Plasma Physics Research Center, Science and Research Branch, Islamic Azad University, Tehran, Iran
- 31: Also at Università degli Studi di Siena, Siena, Italy
- 32: Also at Purdue University, West Lafayette, USA
- 33: Also at International Islamic University of Malaysia, Kuala Lumpur, Malaysia
- 34: Also at Malaysian Nuclear Agency, MOSTI, Kajang, Malaysia
- 35: Also at Consejo Nacional de Ciencia y Tecnología, Mexico city, Mexico
- 36: Also at Warsaw University of Technology, Institute of Electronic Systems, Warsaw, Poland
- 37: Also at Institute for Nuclear Research, Moscow, Russia
- 38: Also at St. Petersburg State Polytechnical University, St. Petersburg, Russia
- 39: Also at National Research Nuclear University 'Moscow Engineering Physics Institute' (MEPhI), Moscow, Russia
- 40: Also at California Institute of Technology, Pasadena, USA
- 41: Also at Faculty of Physics, University of Belgrade, Belgrade, Serbia
- 42: Also at Facoltà Ingegneria, Università di Roma, Roma, Italy
- 43: Also at National Technical University of Athens, Athens, Greece
- 44: Also at Scuola Normale e Sezione dell'INFN, Pisa, Italy
- 45: Also at University of Athens, Athens, Greece
- 46: Also at Institute for Theoretical and Experimental Physics, Moscow, Russia
- 47: Also at Albert Einstein Center for Fundamental Physics, Bern, Switzerland
- 48: Also at Gaziosmanpasa University, Tokat, Turkey
- 49: Also at Adiyaman University, Adiyaman, Turkey
- 50: Also at Mersin University, Mersin, Turkey
- 51: Also at Cag University, Mersin, Turkey
- 52: Also at Piri Reis University, Istanbul, Turkey

-
- 53: Also at Ozyegin University, Istanbul, Turkey
 - 54: Also at Izmir Institute of Technology, Izmir, Turkey
 - 55: Also at Istanbul Bilgi University, Istanbul, Turkey
 - 56: Also at Marmara University, Istanbul, Turkey
 - 57: Also at Kafkas University, Kars, Turkey
 - 58: Also at Yildiz Technical University, Istanbul, Turkey
 - 59: Also at Hacettepe University, Ankara, Turkey
 - 60: Also at Rutherford Appleton Laboratory, Didcot, United Kingdom
 - 61: Also at School of Physics and Astronomy, University of Southampton, Southampton, United Kingdom
 - 62: Also at Instituto de Astrofísica de Canarias, La Laguna, Spain
 - 63: Also at Utah Valley University, Orem, USA
 - 64: Also at University of Belgrade, Faculty of Physics and Vinca Institute of Nuclear Sciences, Belgrade, Serbia
 - 65: Also at Argonne National Laboratory, Argonne, USA
 - 66: Also at Erzincan University, Erzincan, Turkey
 - 67: Also at Mimar Sinan University, Istanbul, Istanbul, Turkey
 - 68: Also at Texas A&M University at Qatar, Doha, Qatar
 - 69: Also at Kyungpook National University, Daegu, Korea